Applied Thermal Engineering 258 (2025) 124593

Contents lists available at ScienceDirect

Applied Thermal Engineering

journal homepage: www.elsevier.com/locate/apthermeng

Research Paper

Techniques to mitigate membrane displacement for vacuum-membrane solar-dish facets

Duncan S. McGee, Willem G. le Roux *

Department of Mechanical and Aeronautical Engineering, University of Pretoria, Hatfield, Pretoria 0028, South Africa

ARTICLE INFO

Keywords:
Vacuum-membrane
Concentrating solar power
Solar dish
Concentrator
Control system
Focus control

ABSTRACT

The prospects of a multifaceted vacuum-membrane solar dish concentrator are considered in this work. The membrane depths of these facets can shift slightly due to varying ambient conditions throughout an operational day, leading to major focal point shifts and a reduced overall efficiency. The purpose of this work was to experimentally investigate different methods of membrane displacement mitigation. A controlled-environment (indoor) enclosure was employed to examine the effects of static ambient conditions, allowing for the independent manipulation of the surrounding pressure and temperature. Various manufacturing techniques were also investigated within the controlled-environment enclosure, which included alterations in pretension, changes in membrane thickness and adjustments to overall facet sizes. Furthermore, outdoor tests were conducted to determine how solar radiation and convection affected membrane displacement as well as to investigate the performance of various membrane depth control strategies using an Arduino Uno microcontroller. The indoor results showed that opting for a small facet would minimize membrane displacement. The results were supported by material tests and a finite element analysis. The outdoor test results indicated that solar radiation and wind affected the internal temperature and consequently also affected the membrane depth. Furthermore, a focus control system maintaining a constant differential pressure across the membrane achieved the required accuracy of ±2 mm membrane displacement limitation. However, another focus control system consisting of a Hall effect module actively monitoring membrane depth emerged as the most effective, with an increase of about 0.09 mm and a decrease of approximately 0.02 mm from an initial depth of 10 mm. This level of stability with a focus control system will ensure that the facet maintains a consistent optical performance, ultimately advancing the reliability and efficiency of low-cost vacuum-membrane technology.

1. Introduction

The sun provides an abundant source of energy that can be harnessed through various methods, including concentrated solar power (CSP) systems. CSP is a growing but expensive alternative energy resource technology. Its high cost is mainly due to high-precision solar concentrators that are required to obtain acceptable operating thermal efficiencies. Murphy [1] stated that the initial cost was estimated to be about 55 USD/m^2 for glass-and-metal heliostats and 20 USD/m^2 for the reflective membrane and support frame design.

A small-scale CSP dish system, Solar Turbo Combined Heat and Power (ST-CHP) was recently demonstrated at the University of Pretoria to generate electrical power and process heat using a micro gas turbine [2]. As indicated in Fig. 1, a multifaceted vacuum-membrane solar dish was constructed from reflective membranes adhered to the rim of commercially available elliptical satellite television antennas (80 cm), due to the low-cost and light-weight advantage of this technology. 0.1-mm-thick EverBright Mirror Film from Sundog Solar Technology [3,4] was used due to its availability and suitability for the intended purpose (outdoors). Swanepoel et al. [2] recommended that actively sensing and controlling the membrane depths throughout an operating day could improve the overall intercept factor to a target value of 90 %, since it was found to be only 64 % (average) for this dish array.

Vacuum-membrane technology has been improved through extensive research over the past years and was first described by Stardobtsev in 1965 [5]. According to Coventry and Andraka [6], Bomin Solar was the first to use large foil membranes in the 1970 s and achieved high concentration ratios. In the late 1980s, a project by Sandia National Laboratories saw the development of single-facet vacuum-membrane-based heliostats by Science Applications International Corporation (SAIC) and Solar Kinetics Inc (SKI) [7]. SAIC and SKI built two facets for

* Corresponding author.
E-mail address: willem.leroux@up.ac.za (W.G. le Roux).

https://doi.org/10.1016/j.applthermaleng.2024.124593
Received 31 January 2024; Received in revised form 8 September 2024; Accepted 9 October 2024
Available online 10 October 2024

Nomenclature

Symbols

A	Area, m^2
C	Polynomial regression coefficient
D	Diameter, m
E	Young's modulus, Pa
Et	Effective mechanical stiffness, N/m
F	Tensile load, N
f	Focal length, m
f_o	Ideal focal length, m
L	Length, m
P	Pressure, Pa
t	Membrane thickness, m
T_o	Geometric induced stiffness due to initial tension, N/m
U	Displacement, m
w	Width, m

Greek

δ	Elongation, m
ε	Strain, m/m
σ	Stress, Pa

Subscripts

0.2	0.2 % stress offset method is applicable
DG	Dog-bone cross-section
m	Membrane
n	Polynomial regression degree
pt	Pretension
R	Radial direction
vm	von Mises
Y	Y-direction

Acronyms

CSP	Concentrating solar power
DHI	Diffuse horizontal irradiance
DNI	Direct normal irradiance
DRO	Digital readout
CFD	Computational fluid dynamics
FEA	Finite element analysis
GHI	Global horizontal irradiance
MD	Machine direction
MDF	Medium density fibreboard
NR	Newton-Raphson
SAIC	Science Applications International Corporation
SAURAN	Southern African Universities Radiometric Network
SERI	Solar Energy Research Institute
SKI	Solar Kinetics Incorporation
ST-CHP	Solar Turbo Combined Heat and Power
TD	Transverse direction

evaluation, with the SKI facet being plastically formed and the SAIC facet elastically formed. The reflective membrane shapes were controlled by a linear actuator on the rear membrane for the SAIC version and a central fan on the front of the heliostat to control the required negative pressure for the SKI version. In parallel with the development of the single facet dishes, Sandia National Laboratories also investigated multifaceted dishes [7] with the potential advantage of being fielded quicker [8]. The multifaceted dish consisted of twelve 3.6-m-diameter vacuum-membrane facets which were designed with two metal membranes stretched over a metal ring, which was about 8 % less efficient than a single-facet design due to increased astigmatic aberrations [8].

Schmitz et al. [9] demonstrated an elliptical vacuum-membrane multifaceted reflector using a silvered aluminium sheet with two membrane thicknesses and found that the thinner aluminium membrane achieved better concentration and intercept factor. According to Dähler et al. [10], this improvement in performance could be attributed to elastoplastic deformation. For a membrane under uniform pressure loading, constant thickness, uniform tension, and supported by a circular frame, the resulting surface would be spherical based solely on equilibrium conditions, as determined by Flügge [11] and Frei [12]. Murphy and Tuan [13] also found that a homogenous and axisymmetric membrane typically assumed a spherical shape. Gehlisch [14,15] and Khoshalm [16] mentioned that if the manufacturing process involved plastically deforming the membrane through large finite deformations to yield a permanent surface, a material with a very low Young's modulus was recommended. This allowed for uniform stress distributions in the yielded areas of the membrane, which would approach a more desired parabolic contoured surface.

Murphy and Tuan [13] determined that a parabolic approximation could be obtained for totally elastic membrane systems, if f_o/D was larger than 2. They also suggested implementing several smaller area facets with large f_o/D ratios to approximate a single large-area parabolic dish facet having a smaller f_o/D, to avoid the problem of differences between spherical and parabolic surfaces. Murphy [17] mentioned that change in focal length was almost entirely due to the nonuniform stress distribution caused by the elastic deformation. Murphy and Tuan [13] determined that a perfect parabolic shape is possible when the Et/T_o ratio was as low as possible, which is possible with a low Young's Modulus, thin membrane, and high membrane pretension. From this, it was evident that the deviation from the ideal parabola decreased with increasing f_o/D and decreasing Et/T_o.

Earlier investigations on vacuum-membrane facets conducted by Roosendaal et al. [18] and Swanepoel et al. [19,2] underscored the critical importance of optical accuracy, as it has a substantial impact on the performance of the collector. This led to the investigations done by McGee et al. [20], where it was evident that the membrane displacement of a vacuum-membrane solar dish facet was highly affected by the change in ambient conditions. The change in membrane depth would change the focal length of a facet and ultimately reduce the efficiency of the CSP system. Investigations conducted by Swanepoel et al. [21] showed that the focal length could change from about 2 m to 8 m when the membrane depth changes from 25 mm to 5 mm for the same size facet (80 cm) used on ST-CHP.

The studies by McGee et al. [20], indicated that the membrane depth moved from about 9.5 mm at an internal temperature of 10 ℃ to a depth of 5.2 mm at a peak internal temperature of 27.5 °C. This excessive membrane displacement would result in the focal point to increase from approximately 4 m to 8 m from the early morning to the middle of the day, as per the findings of Swanepoel et al. [21] and illustrated in Fig. 2. Roosendaal et al. [22] investigated the dependency of the reflector optical performance on facet misalignment and membrane depth with a numerical model. The numerical model aimed at investigating the optical operational boundaries of a multifaceted parabolic vacuum-membrane reflector, assuming an elliptic paraboloid from the photogrammetry of Swanepoel et al. [21]. Roosendaal et al. [22] determined a limit of −2 mm (membrane moving upward) membrane depth change for a targeted minimum intercept factor of 90 % for the solar dish array of ST-CHP [2] (see Fig. 1).

While promising to reduce costs in CSP systems, vacuum-membrane technology still faces challenges. One significant issue is the excessive displacement of the membrane, which can adversely affect optical

accuracy and overall efficiency. Despite this drawback, vacuum-membrane technology offers unique advantages not found in fixed mirror systems. For instance, it allows precise control of the focal point and ability to inflate the vacuum plenum in case of emergencies, effectively defocusing the facet. Focus control systems have therefore been implemented for example by SAIC [23]. This focus control system comprised a steel arm that extended from the facet outer ring to the internal centre of the facet which supported a focussing valve. The airflow of the vacuum pump was then controlled as the front membrane made contact with the valve which maintained the correct membrane position [23]. Schertz et al. [24] mentioned that the valve control concept might not have been the best option because of the need for a steady reference location for the valve. Therefore, SKI applied a focus control system based on sensing and maintaining a differential pressure, where a solenoid valve was opened and closed by two contacts in a pressure switch [24]. According to Grossman et al. [25], the SKI facet encountered some problems with the focusing system when the two facets were compared, due to large pressure fluctuations. Therefore, Schertz et al. [24] recommended that the facet cost and reliability could be improved by instead actively measuring the position of the front membrane to avoid sensitivity to operational and manufacturing variables.

The membrane depths of a multifaceted vacuum-membrane solar dish concentrator as shown in Fig. 1 can shift slightly due to varying ambient conditions throughout an operational day, leading to major focal point shifts and a reduced overall efficiency. The purpose of the current work was therefore to experimentally investigate different methods of membrane displacement mitigation, since analytical work could not accurately represent the real-world conditions of an elliptical vacuum-membrane solar dish facet with a complex geometry. The research sought cost-effective methods through different manufacturing techniques and focus control systems using an Arduino Uno microcontroller. The study also involved investigating the primary reason for membrane displacement through indoor and outdoor experimental work to examine how static and dynamic ambient conditions impacted membrane displacement.

2. Methodology

In the current research, the first aim was to examine how only static ambient conditions impact the displacement of membranes used on vacuum-membrane solar-dishes. A novel controlled-environment enclosure was employed to achieve this goal, allowing for the independent manipulation of the ambient pressure and temperature of a facet. An outdoor test was also conducted on a facet to determine the effects of dynamic ambient conditions on membrane displacement, such as solar radiation and convection. The second aim was to investigate methods to mitigate membrane displacement as much as possible with manufacturing techniques and focus control systems. Various manufacturing techniques were investigated with the objective to identify which manufacturing techniques could effectively minimize membrane depth displacement within the controlled-environment experimental setup. Additionally, the research delved into implementing low-cost focus control systems to further reduce membrane

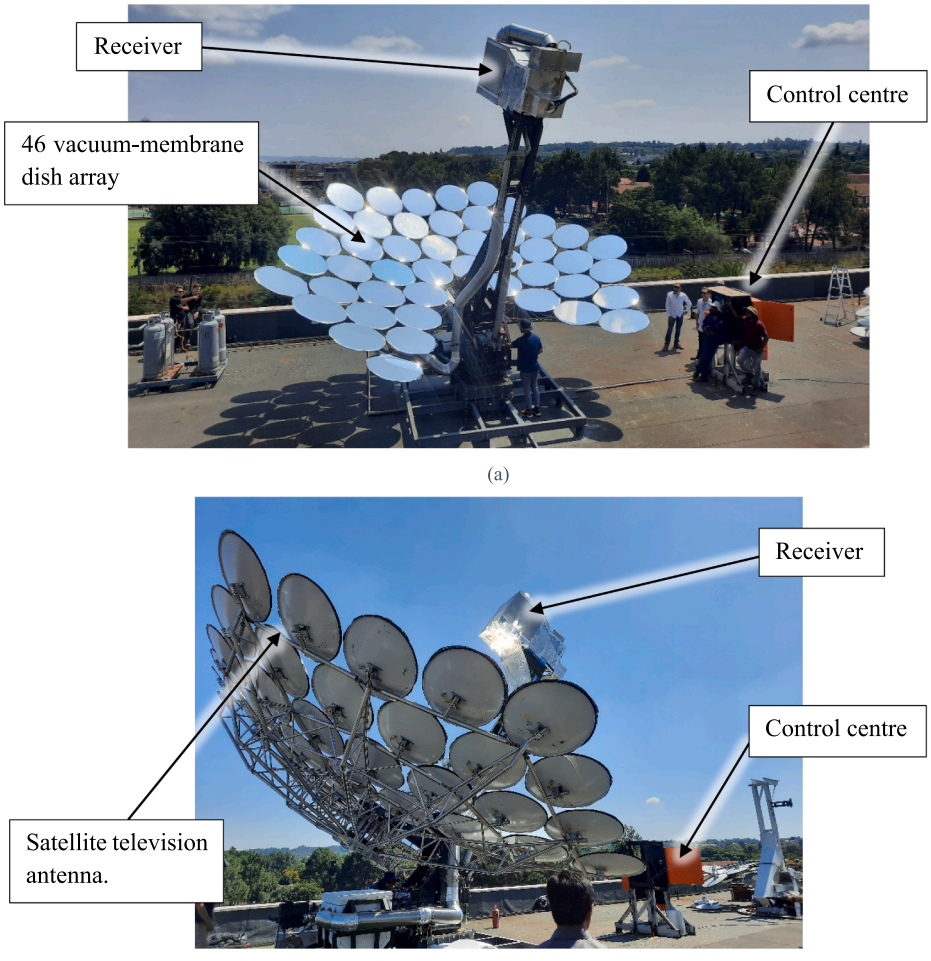

Fig. 1. Multifaceted vacuum-membrane solar-dish setup on the roof of Engineering Building 2 at the University of Pretoria.

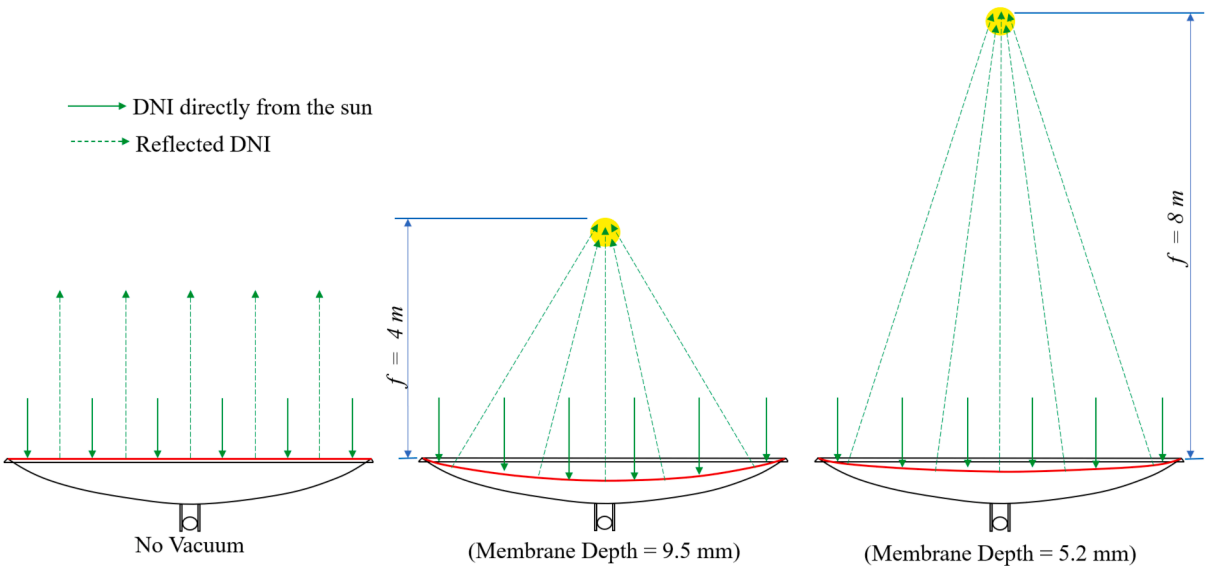

Fig. 2. The effect of changing membrane depth on the focal length.

displacement. This included a control system maintaining a constant differential pressure between the ambient and vacuum plenum of the facet and a control system sensing and maintain the membrane depth. These focus control systems were integrated into real-world testing scenarios to reduce membrane displacement further throughout a typical operating day.

The procedure to achieve the objectives of this research started by first determining the material properties of the chosen reflective membrane material (EverBright Mirror Film from Sundog Solar Technology). This was done with several dog-bone tensile tests to determine the material properties and characteristics within the elastic envelope, as discussed in Section 2.1. The material properties were essential to conduct a plastic-elastic finite element analysis (FEA) to determine the maximum permissible pretension the membrane could handle without permanently deforming, as detailed in Section 2.2. Five facets were then manufactured with different pretensions (based on the FEA findings and the capabilities of the pretension frame), with and without the removable plastic layer, and using different elliptical satellite television antenna sizes. These facets were individually tested in the novel controlled-environment enclosure where the direct ambient pressure and temperature of the facet were altered independently. These tests were conducted several times to ensure good repeatability in the results and to ensure the phenomenon of the membrane behaviour was consistent during all tests. Furthermore, outdoor tests were conducted to test the two different focus control systems, after determining how solar radiation and convection would affect membrane displacement.

2.1. Material tensile tests

A simple dog-bone tensile test was conducted in general accordance with ASTM D882 [26] on the reflective material (with and without the removable plastic layer) to determine the material properties and behaviour until failure or permanent deformation for the FEA study (see Section 2.2). The dimensions of the dog-bone test sample are shown in Fig. 3.

The tensile tests were conducted with a Schenck 100 kN hydraulic actuator setup at the Sasol Laboratory of the University of Pretoria, as shown in Fig. 4. The external 10 kN load cell was calibrated to a value of 500 N/V, and the built-in displacement sensor to a value of 15.057 mm/V.

It was assumed that the reflective material was homogenous [27]. The material was tested in two directions to determine if the material was isotropic or anisotropic. One direction was the longitudinal direction of a facet (machine direction), and the other was the lateral direction of a facet (transverse direction).

The thickness of the reflective material with the removable layer was measured with a micrometer as 0.1 mm and without the removable layer as 0.095 mm. The stress, σ, was determined by dividing the measured tensile load, F, by the initial cross-sectional area of the test sample, as shown in Equation (1), where w was the initial width (20 mm) and t was the initial thickness (with and without the removable plastic layer, 0.1 mm or 0.095 mm) of the test sample.

$$\sigma = \frac{F}{A_{DB}} = \frac{F}{w \times t} \tag{1}$$

The strain, ε, was determined by dividing the elongation, δ, by the initial length, L, of the test section, as shown in Equation (2), where $L = 80$ mm.

$$\varepsilon = \frac{\delta}{L} \tag{2}$$

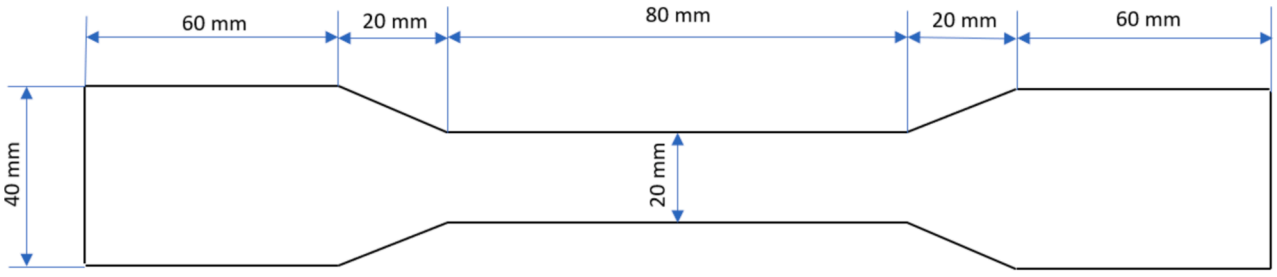

Fig. 3. Top view dimensions of the dog-bone test sample used for the tensile material tests (not to scale).

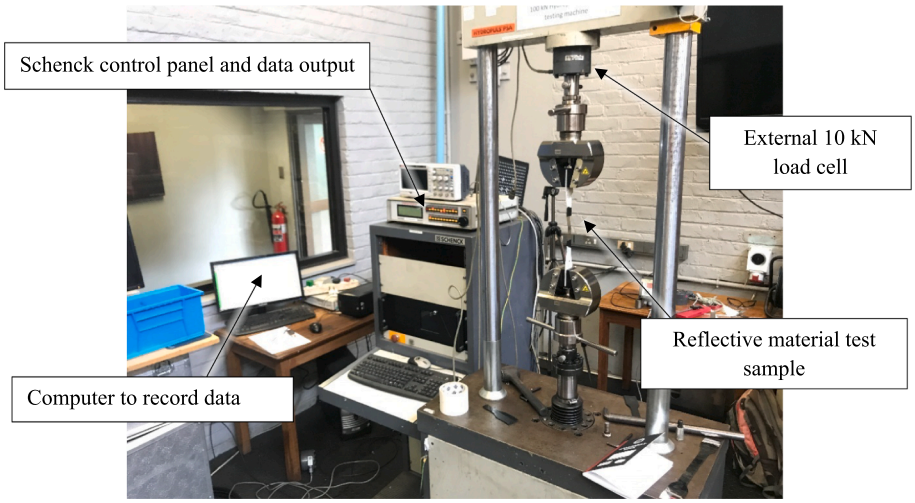

Fig. 4. Tensile material test setup.

A best-fit polynomial regression function was determined and plotted with a Python code to determine the offset yield stress ($\sigma_{0.2}$) and Young's Modulus (E) from Hooke's Law. The regression function (Equation (3)) was then imported to the FEA software to ensure accurate elastic–plastic material properties were considered.

$$\sigma = C_0 + C_1\varepsilon + C_2\varepsilon^2 + \cdots + C_n\varepsilon^n \tag{3}$$

As a conservative approach, the coefficients of the polynomial regression terms of the thinner material (0.095 mm) were considered for the FEA since the thinner reflective material would govern the feasible pretension load.

2.2. Finite element analysis (FEA)

The FEA software used in this analysis was SolidWorks Simulation 2023 x64 SP.2.1 (developed by Dassault Systems) [28] for static nonlinear analyses with the Newton-Raphson (NR) scheme as the iterative solution method [29].

The purpose was only to verify the pretension for the membrane section attached to the elliptical satellite television antenna. The material properties of the reflective material were determined from the tensile material tests mentioned in Section 2.1 and imported to the FEA studies as a von Mises plasticity material model for ductile and isotropic materials, using the determined polynomial regression equation (Equation (3)) of the material. A Poisson's ratio of 0.38 was assumed for the material, which is the value for a similar polymer-based reflective material, commercially known as Mylar [30]. The acceptance criteria of these studies were identified as any pretension loads that would not cause permanent deformation while also considering the effects of applying a vacuum (which would add additional radial load on the membrane).

To determine the effects of pretension on different membrane sizes, two membrane sizes were also analysed, namely the 75 cm [31] and 80 cm [32] membranes, which correspond to the Ellies satellite antenna dish sizes (see Fig. 5).

Two load cases were considered for both membrane sizes with a thickness of 0.095 mm. The first load case was to determine the radial force produced due to the vacuum pressure effects. This load case was conducted by constraining the outer edge of the quarter ellipse vertically and radially from the centre, as shown in Fig. 6. A uniformly increasing pressure was applied to the shell face starting at 0 Pa and moving to a vacuum pressure of 100 Pa (gauge). The reaction force at the outer edge was monitored as an additional radial load. The primary purpose of this load case was to verify that the deformed membrane had a parabolic shape and that the displacement at a specific internal pressure and at

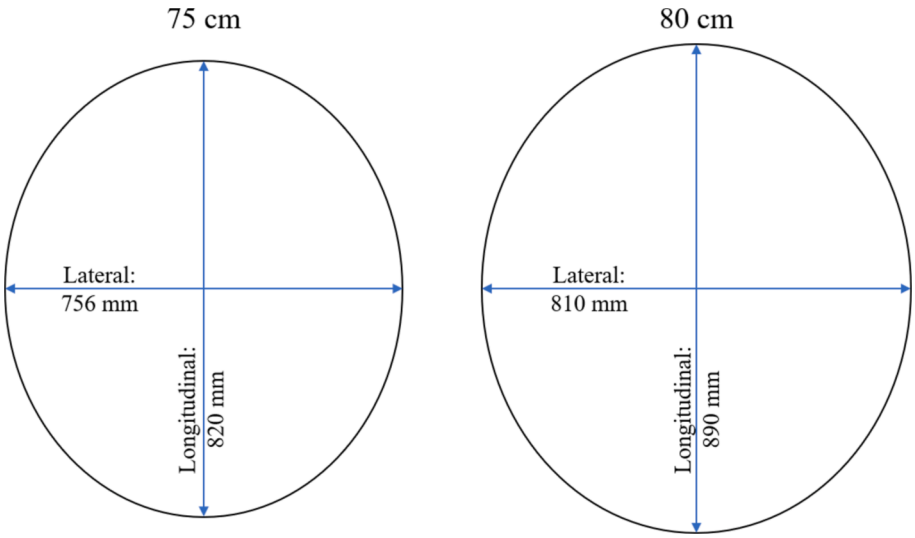

Fig. 5. Membrane sizes considered for the different satellite antenna dishes.

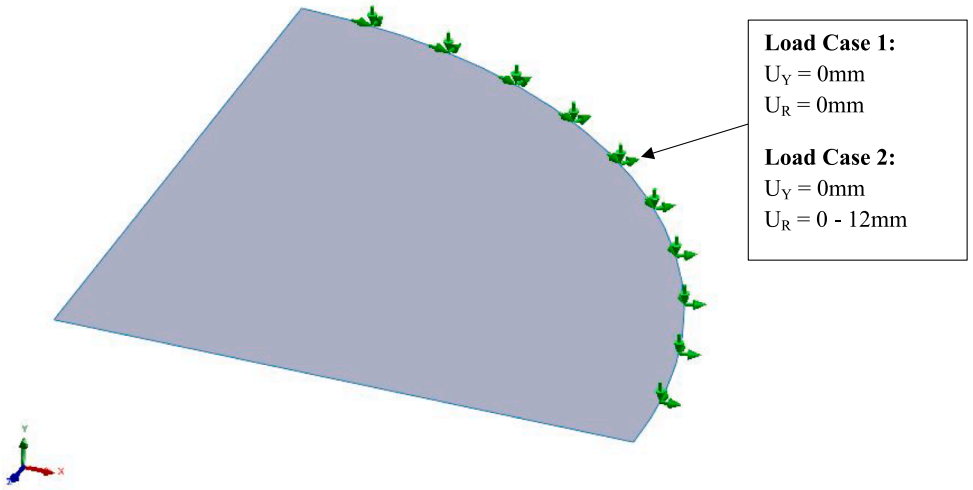

Fig. 6. Applied outer edge boundary conditions for both load cases.

room temperature was the same as found by experiments done by McGee et al. [20]. This would indicate whether the applied FEA method was acceptable or not.

The second load case was to determine the maximum allowable pretension before the material would yield and was done by constraining the outer edge of the quarter ellipse vertically with a uniformly increasing radial displacement starting at 0 mm to a maximum displacement of 12 mm outward at the end of the study, as shown in Fig. 6. The reaction force at the outer edge was then monitored as the pretension load during the radially applied displacement.

The shell models were meshed using second-order triangular shell elements with six nodes per element and six degrees of freedom per node. Only the FEA stress and displacement plots for the larger membrane (80 cm) are illustrated since this was the size used on the ST-CHP system [2].

2.3. Controlled-environment experimental setup

A controlled-environment enclosure (see Fig. 7) was constructed from 30-mm-thick medium density fibreboard (MDF) with a top removable 3-mm-thick acrylic hatch for visibility which was bolted closed when the internal pressure of the enclosure was altered. The MDF enclosure had an internal size of 1470 mm × 1470 mm × 422 mm. Below the enclosure were two 1/4-inch solenoid valves that either allowed air from a high-pressure source into the enclosure to increase the internal pressure or allowed a vacuum pump with a reservoir to extract air from within the enclosure to decrease the internal pressure. The solenoid valves were controlled with an Arduino Uno microcontroller.

A heater with a built-in fan was placed inside the enclosure and controlled with a Delta DTA4848 temperature controller and its own

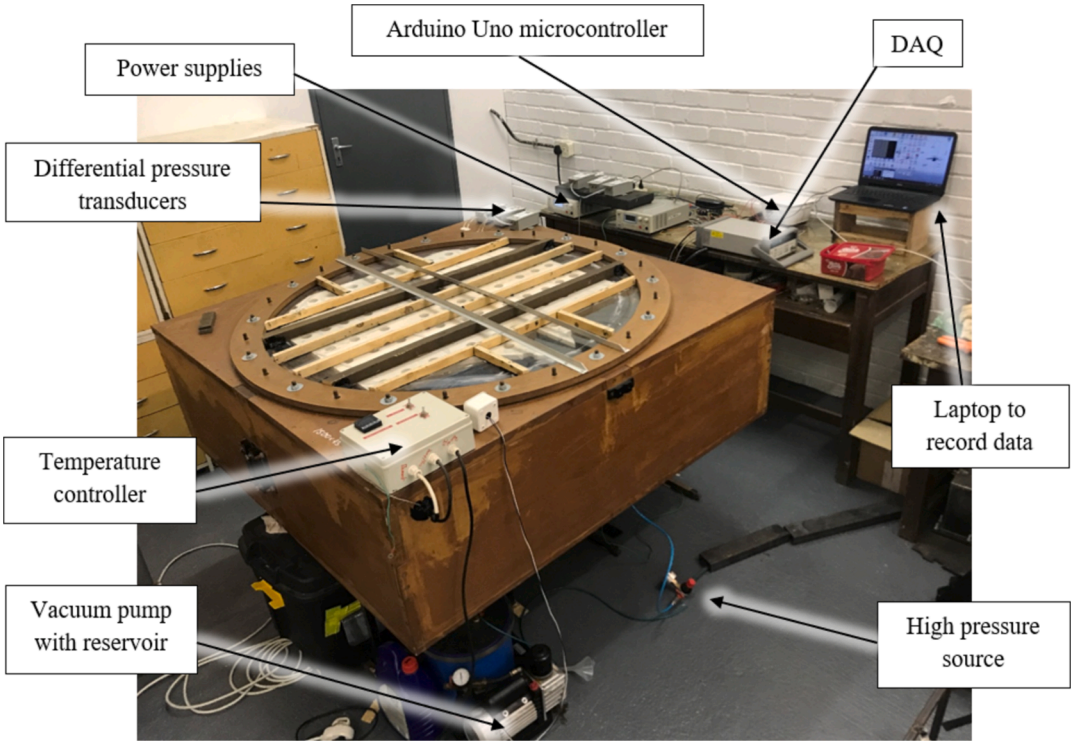

Fig. 7. Controlled-environment experimental setup (outside view) in the Wind Tunnel Laboratory at the University of Pretoria.

thermocouple in front of the fan. A vacuum-membrane solar dish facet mounted in a specially designed frame was placed inside and in the centre of the enclosure before it was closed, as shown in Fig. 8.

The facet support frame was designed to hold the dish on the factory bracket on the back of the dish without the facet touching the support frame anywhere else. This ensured that the facet was mounted as it would be during operation on a small-scaled CSP system, such as ST-CHP shown in Fig. 1b. The top section of the frame that reached over the reflective membrane was designed to cross exactly at the centre of the facet for both large (80 cm [32]) and small (75 cm [31]) elliptical satellite antennas. At this cross was an aluminium guide, guiding a plastic rod up or down as the membrane expanded or contracted due to volume changes of the vacuumed cavity. Three permanent magnets were mounted on the other end of the plastic rod, which were directly below a Hall effect module mounted to the top section of the support frame. The calibrated Hall effect module measured the analogue signal of the magnetic strength in volts.

Five different vacuum-membrane facets were manufactured using EverBright mirror film, then tested in the controlled-environment setup to evaluate how each facet would behave. Each facet with either a different pretension, size (since smaller facet will also result in a better local f/D ratio [13]), or thickness (with or without the removable plastic layer) was tested in the controlled enclosure individually. The Young's Modulus (E) of the two thicknesses were determined with tensile tests in general accordance with ASTM D882 [26] (see Section 3.1), where $E =$ 2.96 GPa without the removable plastic layer and $E = 3.52$ GPa with the plastic layer. The large (80 cm) and small (75 cm) elliptical facets had a circumference of 2672 mm and 2477 mm, respectively. A summary of the different facets is listed Table 1.

A finite element analysis (FEA) was conducted with the measured material properties of the reflective membrane to ensure the membrane would not be permanently deformed when pretensioned to specific values, as discussed in Section 2.2.

The ambient conditions outside the controlled enclosure were monitored to understand how the direct ambient conditions of the facet inside the enclosure were altered. The ambient temperature was measured with a Type-T thermocouple connected to a data acquisition device (DAQ) and the ambient pressure was measured with a BMP280 barometric pressure module connected to an Arduino Uno microcontroller. The differential pressure between ambient and the inside of the enclosure was measured with an Omega PX277 differential pressure transducer connected to the DAQ. With this, the direct ambient conditions of the facet were determined by adding or subtracting the differential pressure transducer reading from the barometric sensor reading.

Table 1
Different facets tested in the controlled-environment enclosure.

Facet Number	1	2	3	4	5
Satellite antenna size [cm]	75	75	75	75	80
Applied pretension mass [kg]	10.85	56.1	80.88	10.85	56.1
Thickness [mm]	0.095	0.1	0.1	0.1	0.1
Pretension (T_o) [N/m]	42.96	222.14	320.26	42.96	205.91
Et/T_o ratio	6545	1584	1099	8193	1709

As shown in Fig. 9, the internal temperature of the enclosure was also measured with a Type-T thermocouple placed on top of the facet support frame as close as possible to the centre of the enclosure. The membrane depth was measured with the Hall effect module. The temperature inside the facet was also measured with a Type-T thermocouple connected with a removable coupling at the bottom of the facet. The differential pressures inside and outside of the facet were also measured with an Omega PX277 differential pressure transducer to determine the internal pressure of the facet. All instrumentation measuring the facet and enclosure conditions were connected to the DAQ which collected data every second. See Section 2.5 for more detail on the sensor calibration and parameters.

2.3.1. *Pressure difference test methodology (simulating a change in ambient pressure)*

A facet was placed inside the controlled-environment enclosure, where the membrane depth was set to approximately 10 mm at the centre of the parabolic shape. The enclosure lid was then bolted shut to ensure a good seal. Two separate tests were conducted where the direct ambient pressure of the facet was either decreased or increased. The Arduino Uno microcontroller activated a relay module which opened a solenoid valve in the piping between the enclosure and either the high-pressure source or the vacuum pump reservoir, which increased or decreased the gauge pressure inside the enclosure. The pressure was increased or decreased until the differential pressure transducer between the internal and external of the enclosure measured about 500 Pa, which then triggered the microcontroller to keep the pressure constant for 20 s by either opening the solenoid valve of the vacuum pump or high-pressure source, depending on how the pressure had to be adjusted

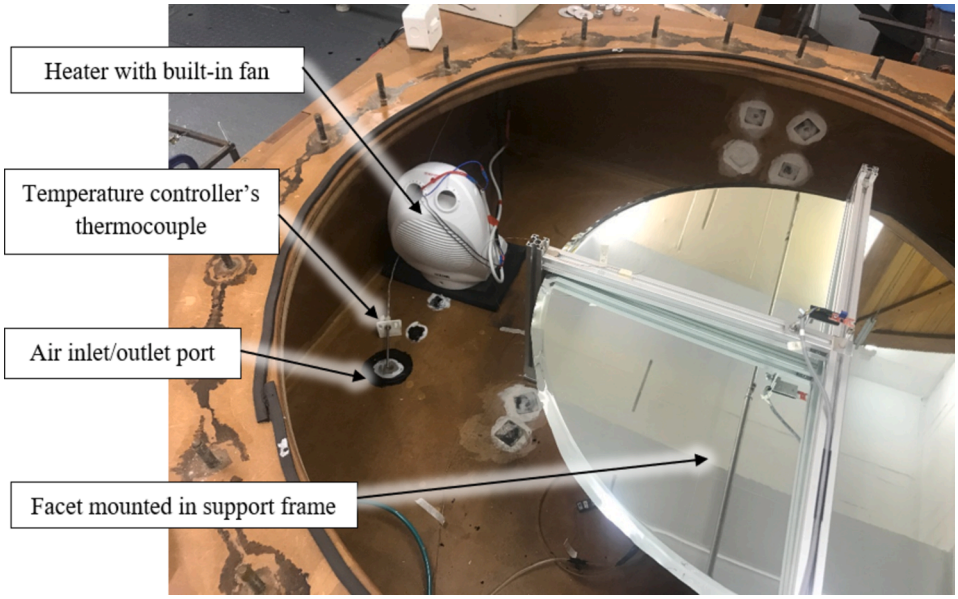

Fig. 8. Controlled-environment experimental setup (inside view).

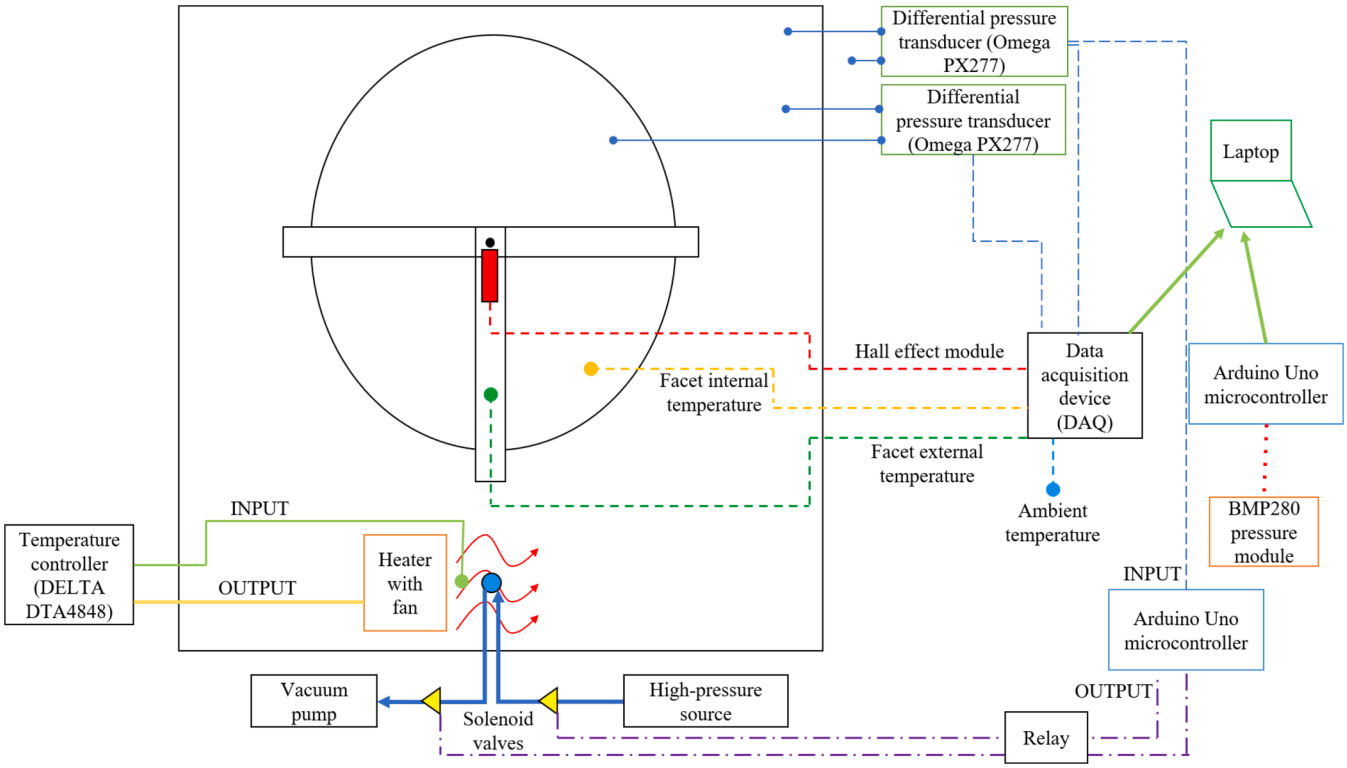

Fig. 9. Controlled-environment enclosure experimental setup schematic.

to keep the enclosure pressure constant. After the 20 s, the microcontroller opened the solenoid valve of the vacuum pump or the high-pressure source to depressurise or pressurize the enclosure back to the initial internal enclosure pressure.

2.3.2. *Temperature difference test methodology (simulating a change in ambient temperature)*

A facet was placed inside the controlled-environment enclosure, where the membrane depth was set to approximately 10 mm at the centre of the parabolic shape. The enclosure lid was only rested onto the protruded bolts, allowing for the tests to be done at ambient pressure. The temperature controller was activated and switched the heater and fan inside the enclosure on. The heater (excluding the fan) was switched on and off constantly for 25 min until the direct ambient temperature of the facet was about 45 ℃. After the 25 min, the heater and fan were switched off and the test was left to monitor the conditions until the temperature reached a constant room temperature again.

2.4. *Outdoor experimental setup*

The outdoor tests were conducted on the roof of the Engineering 2 Building at the University of Pretoria (see Fig. 10). The facet with its support frame was placed at an area on the roof where there was direct sunlight from sunrise to sunset during the wintertime. The facet was

Fig. 10. Outdoor test experimental setup.

stationary and did not face the sun.

The outdoor test (see Fig. 11) was conducted only on Facet 4 (see Table 1 for more detail). The ambient temperature was measured with a Type-T thermocouple connected to a DAQ and the ambient pressure was measured with a BMP280 barometric pressure module connected with an Arduino Uno microcontroller. The differential pressure between ambient and the inside of the facet was measured with an Omega PX277 differential pressure transducer connected to the DAQ.

As shown in Fig. 11, the ambient temperature was also measured with a Type-T thermocouple placed on top of the facet support frame. The membrane depth was measured with the Hall effect module. The temperature inside the facet was also measured with a Type-T thermocouple connected with a removable coupling at the bottom of the facet. All instrumentation measuring the facet internal and ambient conditions were connected to the DAQ and collected data every second.

2.4.1. Outdoor test methodology without a focus control system

This test aimed to understand the effects of actual outdoor conditions on the membrane displacement during an operating day. The membrane depth of the facet was set to approximately 10 mm at the centre of the parabolic shape, and the facet was left outside on the roof. Additionally, the solar radiation was measured from the Southern African Universities Radiometric Network (SAURAN) weather station [33] on top of the Engineering 1 Building at the University of Pretoria and about 90 m away from the outdoor experimental setup to determine if solar radiation had a direct effect on membrane displacement. The wind speed was also measured from this weather station, but it is important to note that the elevation was about 25 m higher than the experimental setup.

2.4.2. Outdoor test methodology at a constant initial differential pressure

For the first control system, the differential pressure was kept constant to keep the internal gauge pressure constant, which should keep the membrane at the initially set depth of approximately 10 mm during an operating day. The hysteresis on–off controller, keeping the differential pressure constant, consisted of only low-cost components. An Arduino Uno microcontroller with two BMP280 barometric pressure modules as the input had an output signal to a relay module for two 12 V diaphragm air pumps of which one was used as a vacuum pump (see Fig. 11).

The BMP280 barometric pressure sensors were placed in a 3D-printed coupling which was placed through a hole on the backside of the satellite antenna and sealed with silicon adhesive (see Fig. 12). One sensor was inside the satellite antenna and the other on the outside. Both sensors were covered to reduce the effects of possible direct wind altering the pressure reading, while the small openings on the covers allowed the sensors to still monitor the static pressure. The total cost of the focus control system at the time of the study was 29.34 USD.

After the membrane depth was set to approximately 10 mm at the centre of the parabolic shape, the microcontroller was switched on which recorded the initial differential pressure as the set point. For every second after the start of the controller, the differential pressure was recorded and compared with the initial value. A 0.1 % error was allowed to ensure that the pumps were not overburdened due to possible noise in the pressure sensor readings.

2.4.3. Outdoor test methodology at a constant membrane depth

The hysteresis on–off controller, keeping the membrane depth constant consisted of the Arduino Uno microcontroller with the Hall effect module as the input, together with an output signal to a relay module for two 12 V diaphragm air pumps of which one was used as a vacuum pump (see Fig. 13). After the membrane depth was set to approximately 10 mm at the centre of the parabolic shape, the microcontroller was switched on which recorded the initial Hall effect analogue reading as the set point. For every second after the start of the controller, the Hall effect reading was recorded and compared with the initial value. A 0.5 % error was allowed to ensure that the pumps were not overburdened due to possible noise in the Hall effect sensor readings. The total cost of this focus control system at the time of the study was about 28.83 USD.

2.5. Sensor calibration and parameters

The type-T thermocouples were calibrated for a range from 10℃ to 40℃ in increments of 1℃ in a thermostatic bath. The Omega PX277 differential pressure transducers were calibrated by first configurating it to measure a maximum differential pressure of 937.5 Pa. The transducers were then switched on with both probes open to the ambient and the voltage reading was recorded as the 0 Pa differential pressure value. The one probe of the transducer was then pressurized to the maximum

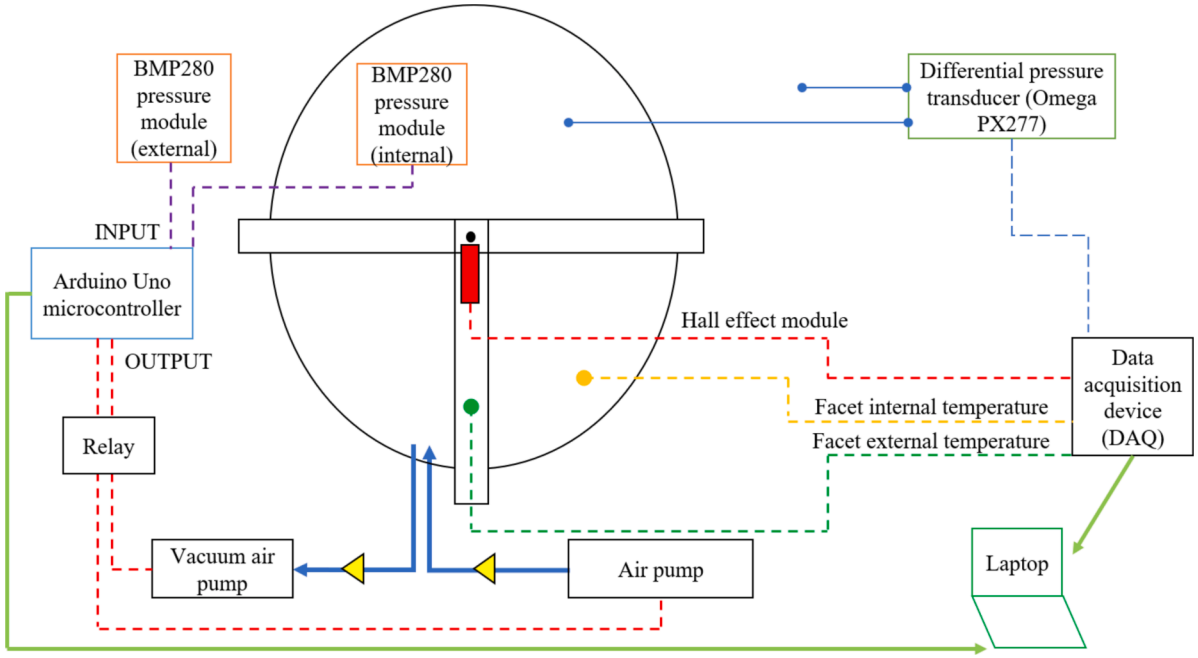

Fig. 11. Outdoor experimental setup schematic (hysteresis on–off control system used to control the differential pressure).

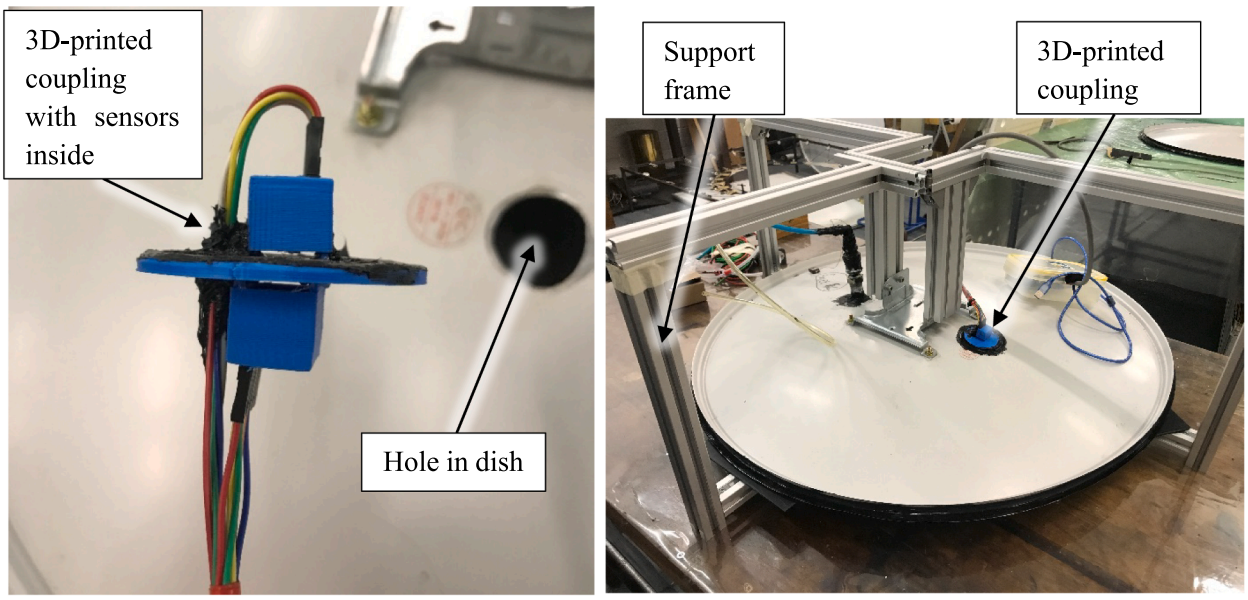

Fig. 12. (a) The 3D printed coupling for the BMP280 barometric sensors, and (b) the facet mounted in the support frame with the coupling attached to the back.

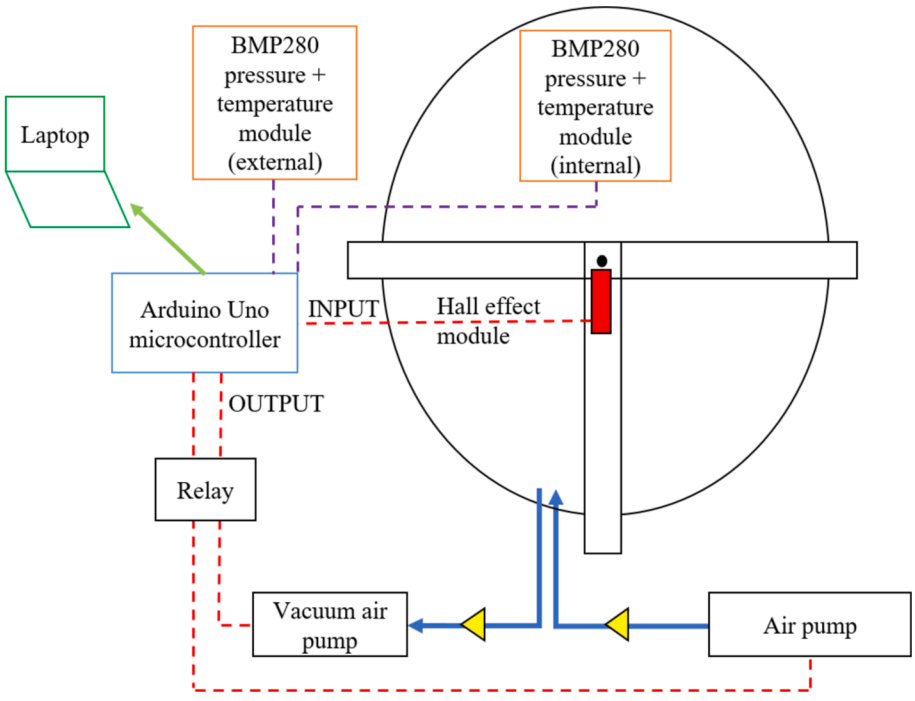

Fig. 13. Schematic of the constant Hall effect module reading experimental setup.

value and the voltage reading was recorded where the differential pressure is 937.5 Pa. This resulted in a calibrated linear function with a differential pressure range of 0 Pa to 937.5 Pa. The BMP280 absolute barometric sensors were not calibrated for at the time of this research, however, according to the manufacturer datasheet [34], the pressure and temperature reading has an accuracy of ±0.12 hPa and ± 1℃, respectively. The Hall effect module was calibrated with a milling machine and digital readout (DRO) at increments of 0.5 mm from 0 mm to 25 mm, which resulted in a function that gave the membrane depth in millimetres from a voltage reading. The repeatability of the measurement was checked by later recording the voltage at random depths and comparing them with the original voltage reading, showing an acceptable repeatability of within ± 0.0001 V. It is important to note that the same sensors were used in all experiments conducted to reduce the error when comparing results between differently manufactured facets or control systems.

3. Results and discussions

3.1. Material tensile test results

Fig. 14 shows that the material exhibited isotropic properties within the elastic range. However, as the stress surpassed the yield point, the material transitioned into anisotropic behaviour within the plastic

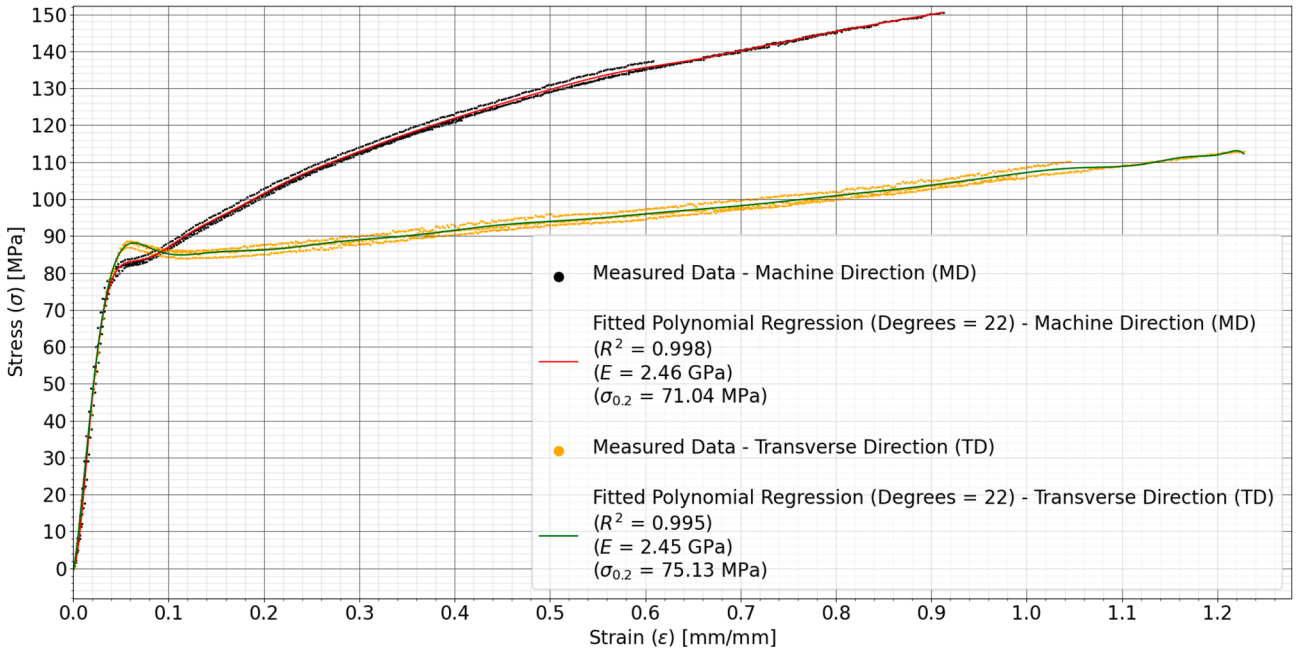

Fig. 14. Stress–strain diagram in two directions and same thickness (0.095 mm) (27 January 2023).

range. This distinction simplified the FEA because the primary concern was the behaviour of the material within the elastic range since a plastically deformed reflective membrane was not desirable for the current facet design in this research.

Fig. 15 shows the behaviour of the material with and without the removeable plastic layer. The reflective membrane with a thicker profile, featuring a removable plastic layer and an overall thickness of 0.1 mm, displayed superior elastic material properties compared to the thinner reflective membrane, which had a thickness of 0.095 mm.

Equation (3), with the coefficients for the polynomial terms, was imported into the elastic plastic FEA studies (see Section 3.2), including a Young's modulus of 2.46 GPa and an offset yield stress of 71.04 MPa, since these were the smallest values obtained, in order to produce conservative results.

3.2. *Finite element analysis results*

In the first load case, the radial reaction load exhibited a linear increase, while the centre vertical displacement of the membrane changed exponentially. This behaviour is illustrated in Fig. 16, with a maximum radial load of 56.1 N for the large membrane at 100 Pa.

The deformed displacement, as depicted in Fig. 17 and Fig. 18,

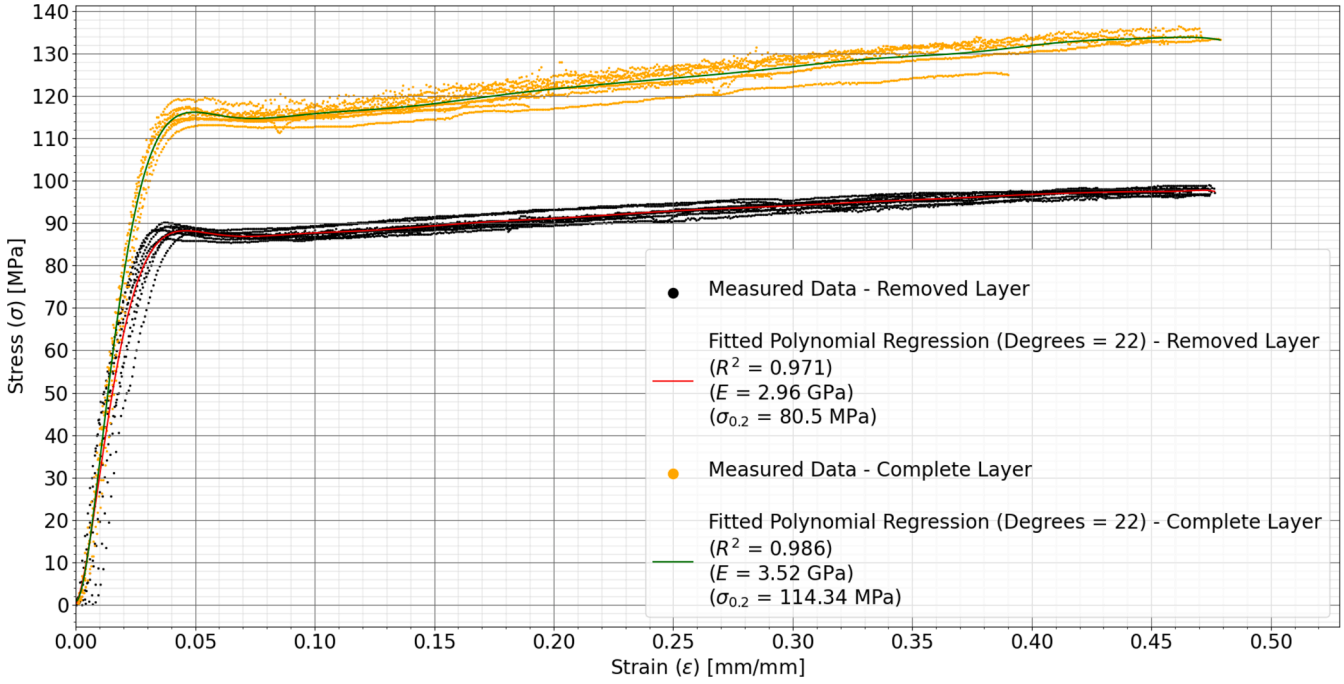

Fig. 15. Stress–strain diagram of the complete reflective membrane material with the removable plastic layer (0.1 mm) and without the removable plastic layer (0.095 mm) and in the transverse direction (22 July 2022).

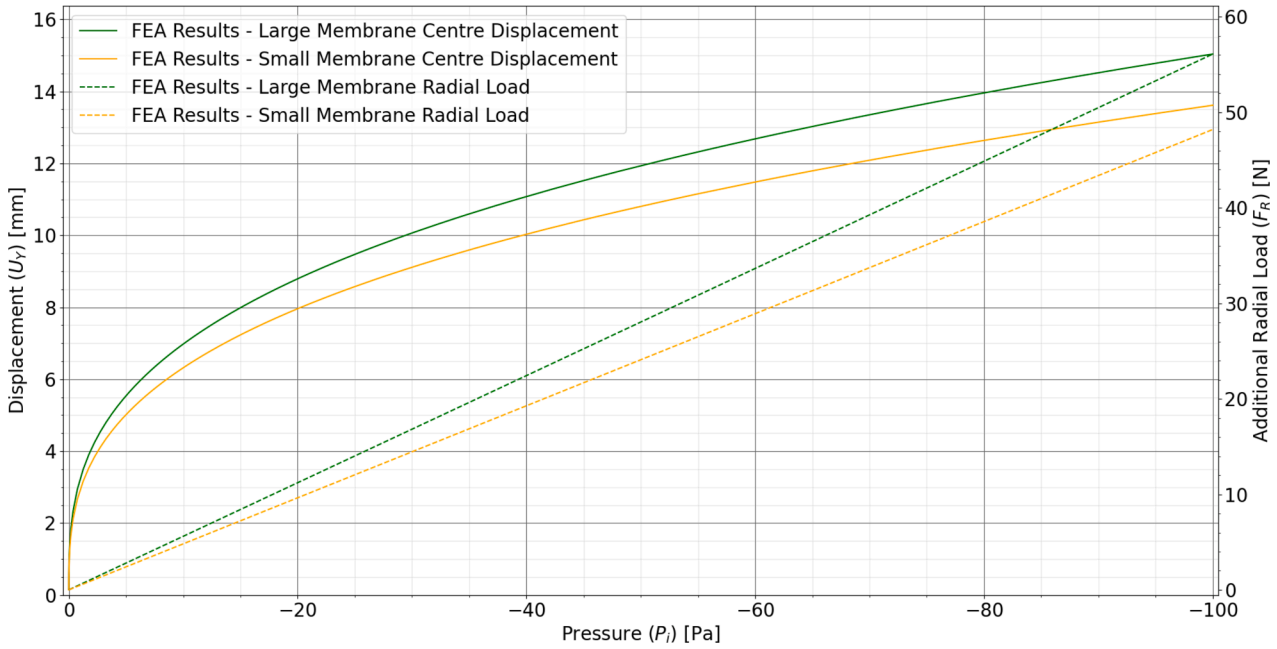

Fig. 16. Centre displacement and additional radial load due to applied pressure for two membrane sizes.

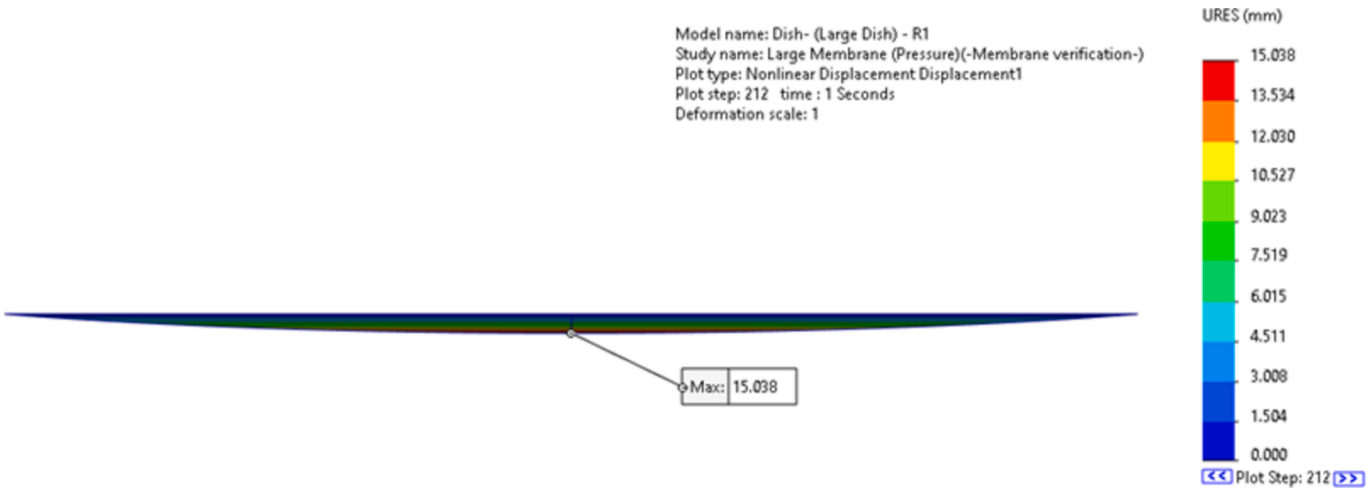

Fig. 17. The side view of the deformed displacement of the 80 cm membrane (Load Case 1).

illustrates that the membrane deformed in a parabolic manner as expected. Research conducted by McGee, et al. [20] established that the membrane depth for an 80 cm facet reached approximately 8.4 mm under an internal vacuum pressure and temperature of around 20 Pa and 20 °C, respectively, at 9:15 in the morning. According to Fig. 16, the vertical centre displacement of the membrane at 20 Pa was 8.8 mm, resulting in a 4.7 % error when compared to the measured displacement. This error suggests that the applied FEA method was deemed acceptable.

Based on the findings in Fig. 16, the smaller membrane would necessitate a higher vacuum pressure for a specific membrane depth than the larger membrane due to its smaller surface area. This also suggested that introducing a vacuum in a vacuum-membrane solar dish would not result in worrisome stress levels. Refer to Fig. 19 for the von Mises stress plot of Load Case 1.

In the second load case, it became evident that the larger membrane exhibited greater pretension capabilities than the smaller one (as depicted in Fig. 20). The results from this study indicated that the maximum equivalent von Mises stress and pretension load increased linearly until the material reached its yield point, corresponding to the uniform rise in radial displacement.

The maximum equivalent von Mises stress was found on the outer edges of the shorter lateral length of the elliptical membrane face, with the minimum stress on the outer edges of the longer longitudinal length of the membrane, as shown in Fig. 21. Fig. 22 indicates that an even radial displacement was applied on the outer edge.

The additional radial load caused by pressure (56.1 N/hPa) was not a cause for concern when compared to the material pretension capabilities since the maximum permissible radial load for both membrane sizes is 16.1 kN. While this load was excessive for the structural integrity of the attachment points on the membrane, the pretension frame, and the satellite antenna dish, it would still result in satisfactory safety margins and an extended creep life when realistic pretension loads are considered. It was determined through initial experimental testing that a pretension force of approximately 810 N could be safely applied before any attachment points on the membrane would experience tearing, which was well below the pretension capabilities determined.

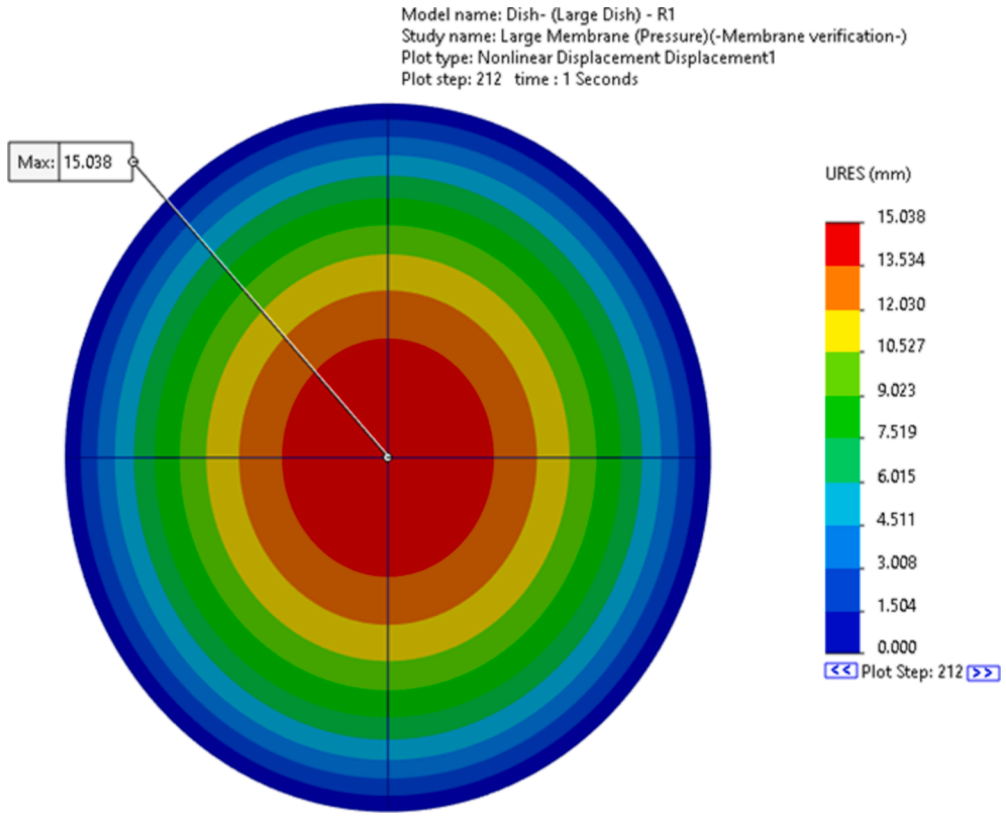

Fig. 18. The depth view of the deformed displacement of the 80 cm membrane (Load Case 1).

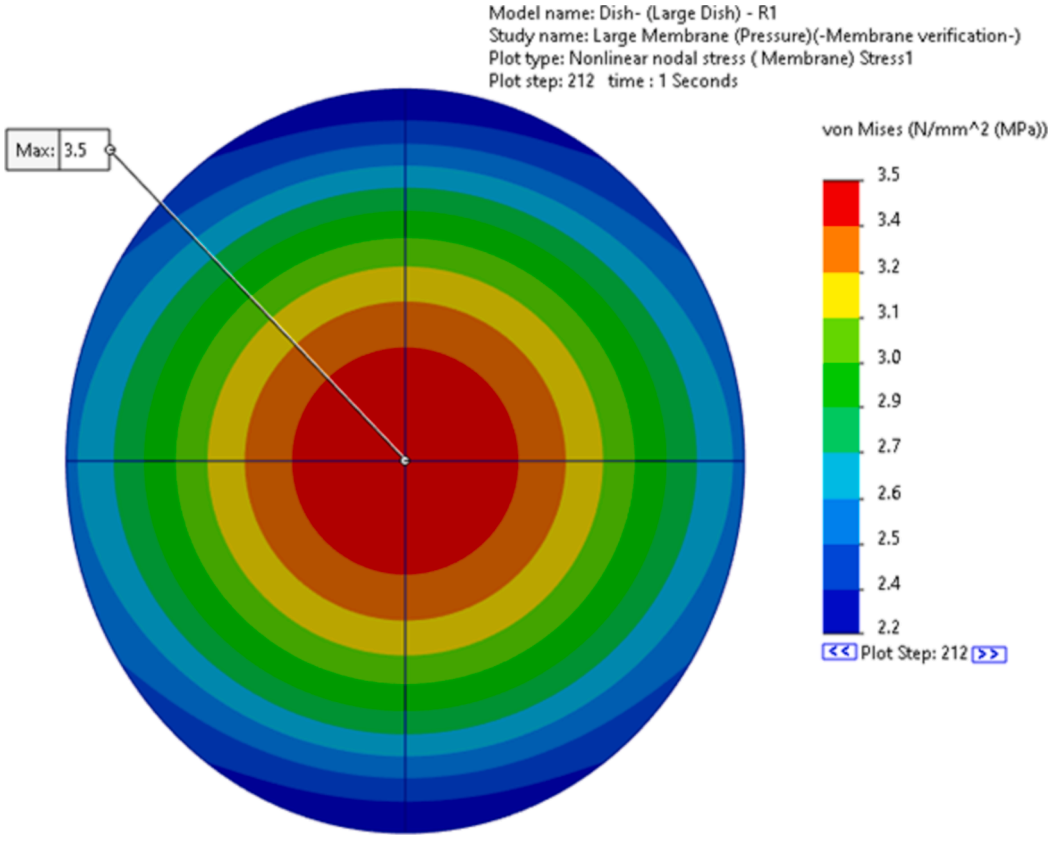

Fig. 19. Von Mises stress plot of the 80 cm membrane – Load Case 1.

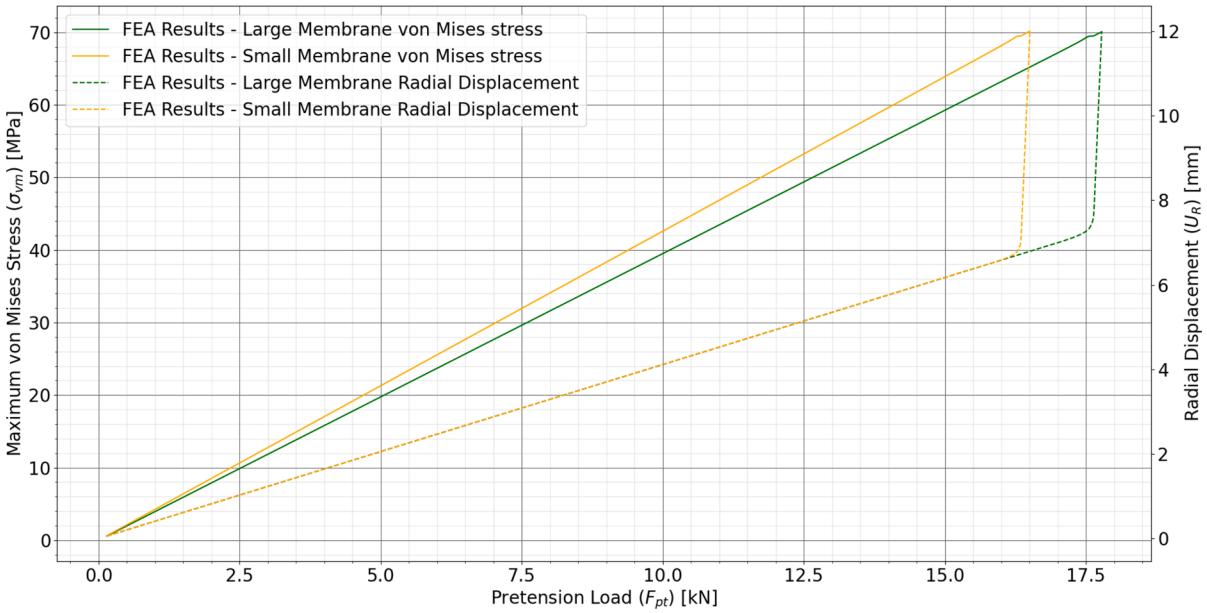

Fig. 20. Maximum von Mises stress and radial displacement due to pretension for two membrane sizes.

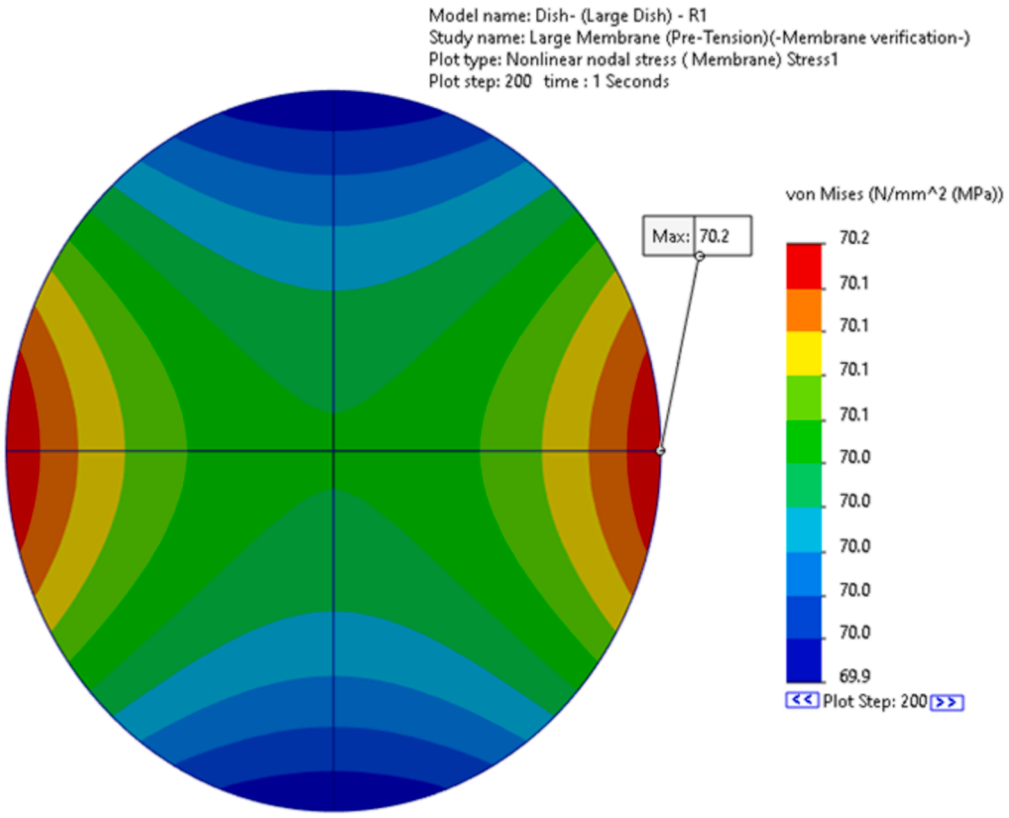

Fig. 21. Von Mises stress plot of the 80 cm membrane – Load Case 2.

3.3. Controlled-environment experimental results (indoor tests)

Five differently-manufactured vacuum-membrane solar dish facets were individually tested within the controlled enclosure, and a summary of the results will be presented in Section 3.3.3 (see Table 2). In the sections below, however, the results are shown in detail for Facet 4.

3.3.1. Pressure difference test results (simulating a change in ambient pressure)

Fig. 23 illustrates the complete process of the test conducted on the facet, wherein the direct ambient pressure was reduced by about 500 Pa. The membrane depth exhibited a linear change, increasing by approximately 0.8 mm as the direct ambient pressure of the facet reached around −500 Pa (g). Linear relationships were clearly depicted in Fig. 24 and Fig. 25, with the pressure decrease and increase periods isolated for

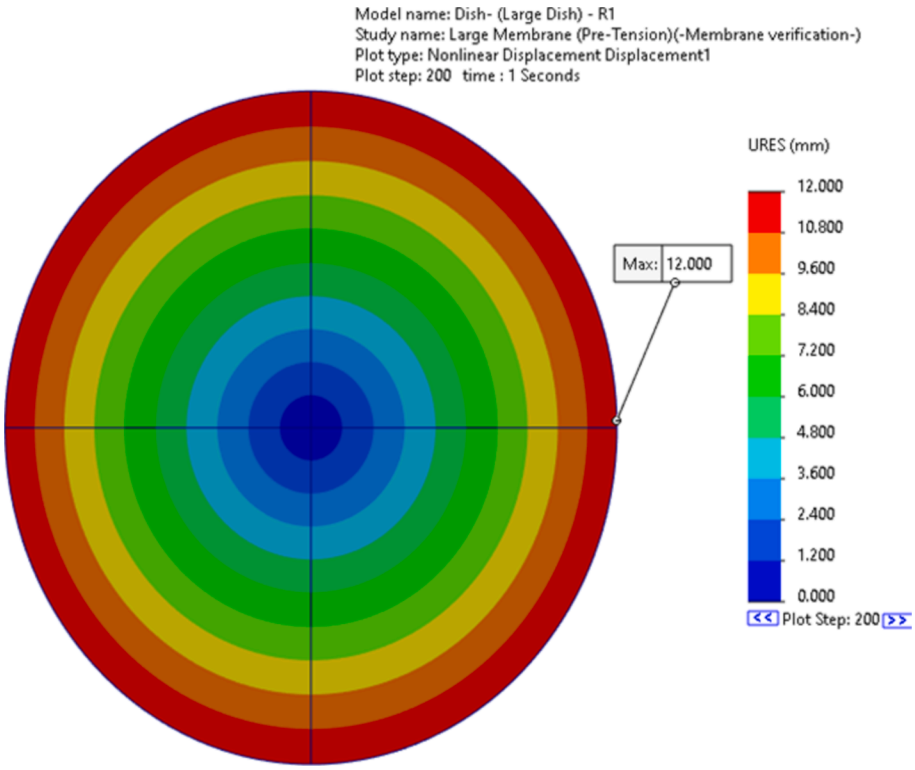

Fig. 22. Displacement (radial) plot of the 80 cm membrane – Load Case 2.

clarity. During the test, a minor decrease in the facet internal and direct ambient temperature was observed because of the pressure decrease, aligning with the principles of the ideal gas law. Furthermore, the internal pressure within the facet exhibited a slight increase when the direct ambient pressure was reduced. This phenomenon could be attributed to the decrease in air particles within the enclosure, exerting less force on the outside surface of the membrane. Consequently, the relatively constant air particles within the facet caused the membrane to move slightly upwards, as the opposing force from the outside diminished.

For the isolated pressure decrease and increase periods of the test, it was observed that the membrane depth deviated slightly from its initial position due to the changes in direct facet ambient pressure, which, in turn, influenced the internal and direct ambient temperature of the facet. However, this deviation was minimal, and a clear linear relationship remained discernible. In Fig. 24, a linear relationship of 0.149 mm/hPa was identified between the membrane displacement and the ambient pressure of the facet. Similar results were observed for the facet internal conditions, where Fig. 25 depicts a linear relationship of 7.488 mm/hPa between the membrane displacement and the internal pressure of the facet.

Fig. 26 illustrates the complete process of the test conducted on the facet while increasing the direct ambient pressure by about 500 Pa. The membrane depth decreased by a total of approximately 0.64 mm until the direct ambient pressure of the facet reached about 500 Pa (g). Linear relationships were clearly depicted in Fig. 27 and Fig. 28, with the pressure increase and decrease periods isolated for clarity. During the period when the direct ambient pressure was increased, there was a slight decrease in the internal pressure of the facet.

Fig. 27 demonstrates a linear relationship of 0.119 mm/hPa between the membrane displacement and the ambient pressure of the facet. It is noteworthy that the effect of decreasing (Section 3.1.1) or increasing (Section 3.1.2) ambient pressure appeared to be almost similar, with a difference of approximately 0.03 mm/hPa (0.15 mm difference over a pressure alteration of 500 Pa). This difference could be due to measuring errors, linear regression errors, or to the slight differences in temperatures during the two tests.

Similar findings were also evident concerning the facet internal conditions, where a linear relationship of 6.444 mm/hPa was established between the membrane and the internal pressure of the facet, as depicted in Fig. 28. Notably, this was approximately 1.044 mm/hPa less than what was determined in the ambient pressure decrease test (Section 3.1.1), which could also be attributed to factors such as rounding errors, the accuracy of the fitted linear regression function, and/or slight temperature fluctuations encountered during the test.

As indicated in Fig. 29 and Fig. 30 the differential pressure had a linear correlation with membrane displacement when the direct ambient pressure of a facet was decreased and increased, respectively. It was determined that this relationship had an average 7.136 mm/hPa linear correlation with minimal differential temperature changes during the tests as indicated in Fig. 31and Fig. 32. As summarized in Table 2, the average correlation between internal pressure and membrane displacement was 6.966 mm/hPa, which is a 2.4 % difference to the correlation between differential pressure and membrane displacement. This indicates that differential pressure correlations are a good variable to investigate for future work but will not add more value to the current objective.

3.3.2. Temperature difference test results (simulating a change in ambient temperature)

Fig. 33 presents the complete test process conducted on the facet, during which the ambient temperature was raised by approximately 20 °C and then allowed to gradually decrease to room temperature. The facet direct ambient temperature quickly rose to about 48 °C, and subsequently, the heater was turned off by the temperature controller to allow the temperature to decrease to about 45 °C. This led to frequent cycling of the heater that was switching on and off over a span of 25 min, as depicted in the figure, resulting in temperature fluctuations. The temperature fluctuations due to the heater was also reflected in the displacement of the membrane, indicating that temperature

Table 2
Comparative summary of the controlled-environment results of different facet types.

	Thin membrane	Large facet	Different pretension facets		
Facet	**1**	**5**	**4**	**2**	**3**
Satellite antenna size [cm]	75	80	75	75	75
Pretension [kg]	10.85	56.1	10.85	56.1	80.88
Thickness [mm] (with or without the removeable plastic layer)	0.095	0.1	0.1	0.1	0.1
Et/T_o ratio	6545	1709	8193	1584	1099
Membrane displacement per ambient pressure change [mm/hPa] (decreased ambient pressure test)	0.145	0.148	0.149	0.138	0.133
Membrane displacement per ambient pressure change [mm/hPa] (increased ambient pressure test)	0.134	0.159	0.119	0.133	0.126
Average membrane displacement per ambient pressure change [mm/hPa]	0.140	0.154	0.134	0.136	0.130
Membrane displacement per internal pressure change [mm/hPa] (decreased ambient pressure test)	10.251	9.955	7.488	6.185	6.584
Membrane displacement per internal pressure change [mm/hPa] (increased ambient pressure test)	9.327	10.159	6.444	5.904	5.904
Average membrane displacement per internal pressure change [mm/hPa]	9.789	10.057	6.966	6.045	6.350
Membrane displacement per ambient temperature change [mm/C] (ambient temperature cooling period)	0.150	0.268	0.169	0.164	0.156
Membrane displacement per internal temperature change [mm/C] (ambient temperature heating period)	0.169	0.221	0.152	0.160	0.158
Membrane displacement per internal temperature change [mm/C] (ambient temperature cooling period)	0.130	0.226	0.135	0.131	0.150
Average membrane displacement per internal temperature change [mm/C]	0.150	0.224	0.144	0.146	0.154

significantly influenced membrane behaviour. Concurrently, the facet internal pressure began to rise immediately when the heater was activated, and it continued to increase throughout the heating period. The membrane depth decreased by approximately 3 mm during this heating phase, lasting until the internal facet temperature reached 41 °C. Both the internal temperature of the facet and the membrane depth exhibited a sudden increase, with minor fluctuations attributed to the heater, until the heater and fan were turned off for the cooling phase of the test. During the cooling phase, the direct ambient temperature and internal pressure of the facet rapidly decreased. Simultaneously, the membrane depth increased swiftly during the initial few minutes, as the conditions both around and inside the facet returned to their initial states.

During the heating phase of the test, Fig. 34 reveals that the direct ambient pressure of the facet exhibited fluctuations of approximately 0.1 hPa. Additionally, it is apparent that the direct ambient pressure decreased by approximately 0.3 hPa during the cooling period. These observations suggested that ambient pressure had a minor influence on the displacement of the membrane depth during this test. Moreover, there was a linear trend in the membrane depth versus ambient temperature during the cooling period, spanning from 35 °C to 26 °C.

Fig. 35 illustrates how the internal pressure of the facet exhibited a sudden increase initially as the internal temperature increased. Once the fluctuations caused by the heater began, the internal pressure displayed a linear increase until the internal temperature reached its peak at 41 °C. This data exhibited less fluctuation because the air inside the facet was not in direct contact with the effects of the heater. At the start of the heating period in this figure, the membrane depth experienced a steep decrease until it reached a depth of 8.7 mm. Following this, the depth fluctuated in a linearly decreasing trend until reaching its minimum depth of 6.8 mm. As the ambient temperature decreased during the cooling period, the membrane depth initially increased suddenly until it reached 8.3 mm, after which it increased linearly until the test concluded.

The nonlinear periods shown in Figs. 30 and 31 are due to the effects of the inconstant rate of change between the internal and external air temperature of the facet. Only sudden changes in ambient or internal temperatures will result in such nonlinear behaviour, which is only expected to happen when a cloud moves over the facet. The nonlinear parts shown in these figures are only an exaggerated effect due to the sudden change in the direct ambient temperature of the facet caused by the heater. However, once a constant rate of change is reached between the internal and external air, the effects are shown to have a linear correlation, which is expected to be the case in normal operating conditions. See Fig. 36 for better clarity on the isolated periods when the facet has a constant rate of change while the direct ambient temperature changed. The linear correlations (mm/°C) in this figure were used to compare the differently manufactured facets in Table 2.

Fig. 36 presents the isolated steady-state heat transfer data from the temperature test. During the heating period, a linear relationship of 0.152 mm/C was identified between the membrane displacement and internal temperature. During the cooling period, a linear relationship of 0.135 mm/C was established between the membrane displacement and internal temperature. Additionally, a linear relationship of 0.169 mm/C was determined between the membrane displacement and ambient temperature during the cooling period.

When isolating the constant rate of change periods of the differential temperature versus membrane displacement in Fig. 37, it was found that there are linear correlations during the heating and cooling periods of the tests. The correlation between differential temperature and membrane displacement was found to be 0.207 mm/C and 0.690 mm/C during the heating and cooling periods, respectively. It was found that the change in differential pressure also had an effect on these correlations since the direct ambient pressure changed during these tests.

Based on the results of Facet 4, it was evident that ambient temperature would exert a more significant influence on membrane displacement compared to ambient pressure during a typical operational day. During a typical winter-day in 2023 in Pretoria, it was expected that ambient pressure would fluctuate by approximately 3 hPa (06:00 to 13:00), while ambient temperature was anticipated to increase by around 15 °C (at 13:00) from an average minimum of 12.8 ℃ (at 06:00) [33]. These fluctuations would lead to a membrane depth change of approximately 0.357 mm due to ambient pressure variations and a much more substantial change of approximately 2.535 mm due to temperature fluctuations, excluding the effects of radiation and convection, which may further contribute to the displacement of the membrane.

3.3.3. *Comparative summary of the controlled-environment results*

When comparing the results of the controlled-environment tests between the large (Facet 5) and small (Facet 2) facets with the same

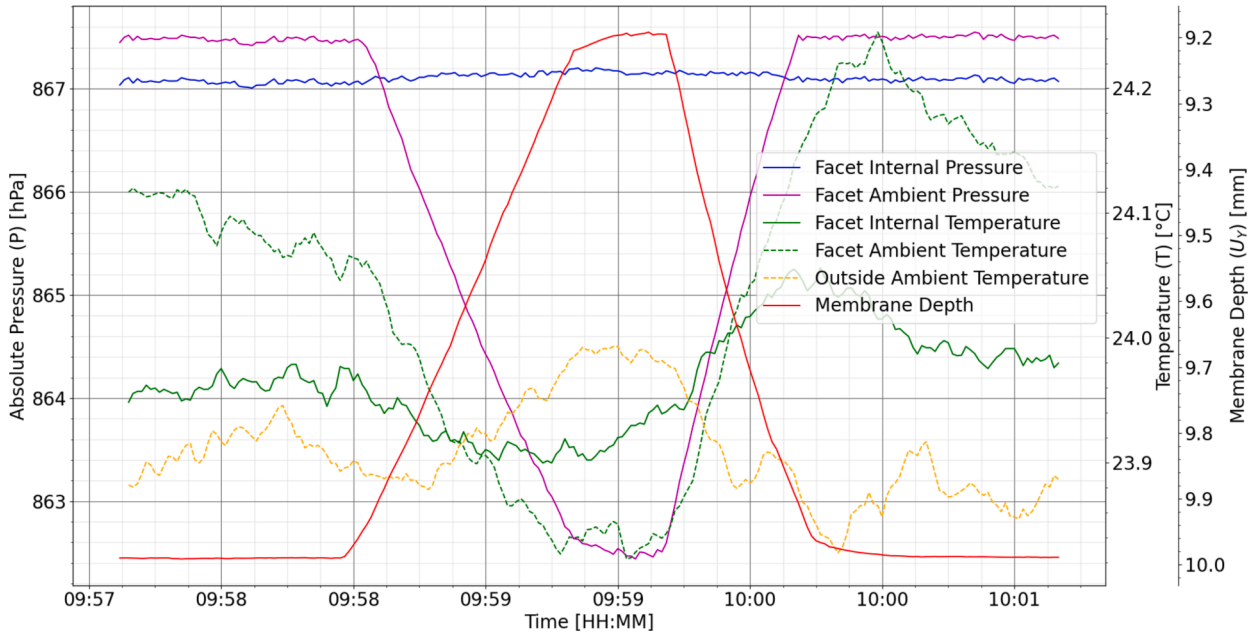

Fig. 23. Decrease in ambient pressure test of Facet 4 (7 May 2023).

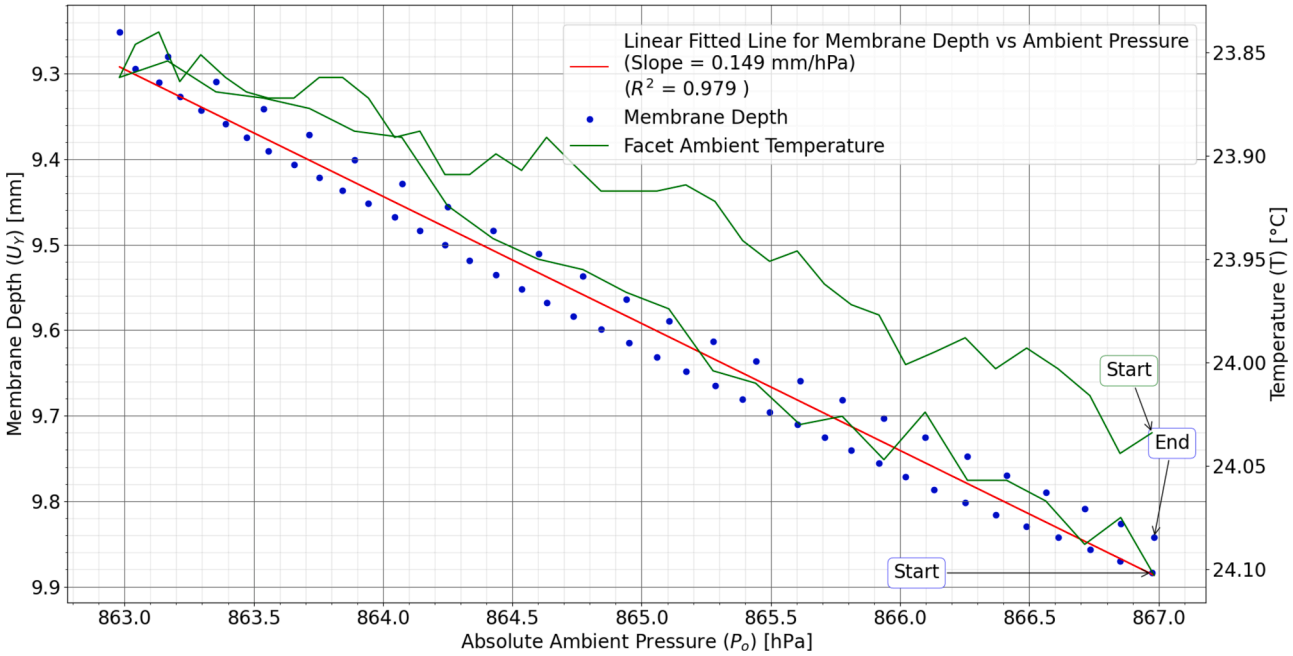

Fig. 24. Membrane depth and internal temperature of Facet 4 versus the decrease ambient pressure (7 May 2023).

pretension, it became evident that the displacement of the membrane due to changing ambient pressure was less pronounced for the smaller facet, as indicated in Table 2. Specifically, the average ambient pressure effect was found to be 0.154 mm/hPa for the large facet and 0.136 mm/hPa for the small facet, reflecting a 13.2 % difference. Additionally, the ambient temperature was found to impact membrane displacement by 0.268 mm/C for the large facet and 0.164 mm/C for the small facet, resulting in a more significant 63.4 % difference. These findings suggest that a smaller facet (with a lower Et/T_o ratio) would experience less membrane displacement during operational conditions compared to a larger facet, which is also an optical advantage. This is likely because a larger facet has more membrane surface area, making it more susceptible to changes in ambient pressure, and the greater number of air particles inside the facet would expand more when heated. Notably, the average internal temperature effect for the larger facet was 53.4 % higher than for the smaller facet.

In contrast, when comparing the results between thick (Facet 4 – with the removable plastic layer) and thin (Facet 1 – without the protective removable layer) membrane facets with the same pretension and size, it was determined that the membrane displacement due to changing ambient pressure was approximately the same for both thicknesses, as displayed in Table 2. The average ambient pressure effect was 0.134 mm/hPa for the thick membrane and 0.140 mm/hPa for the thin membrane, resulting in a minor 4.5 % difference. Regarding the impact of ambient temperature, it was found to be 0.169 mm/C for the thick membrane and 0.150 mm/C for the thin membrane, resulting in a

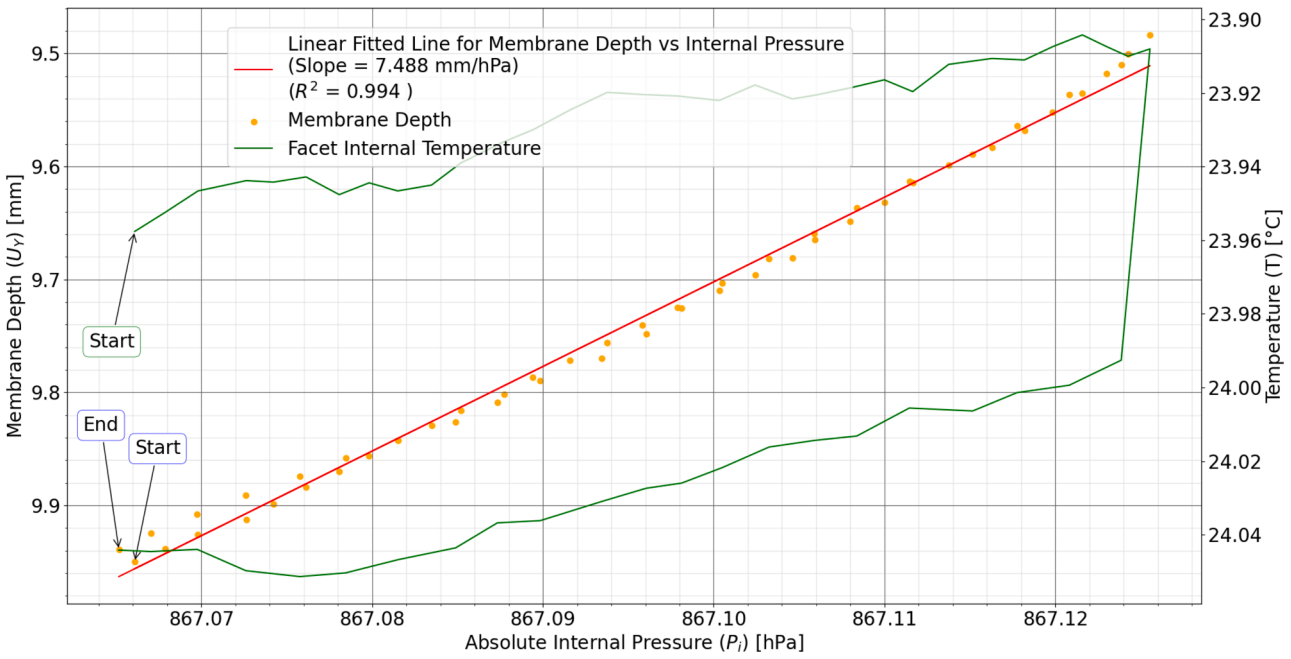

Fig. 25. Membrane depth and internal temperature versus internal pressure of Facet 4 as the ambient pressure decrease (7 May 2023).

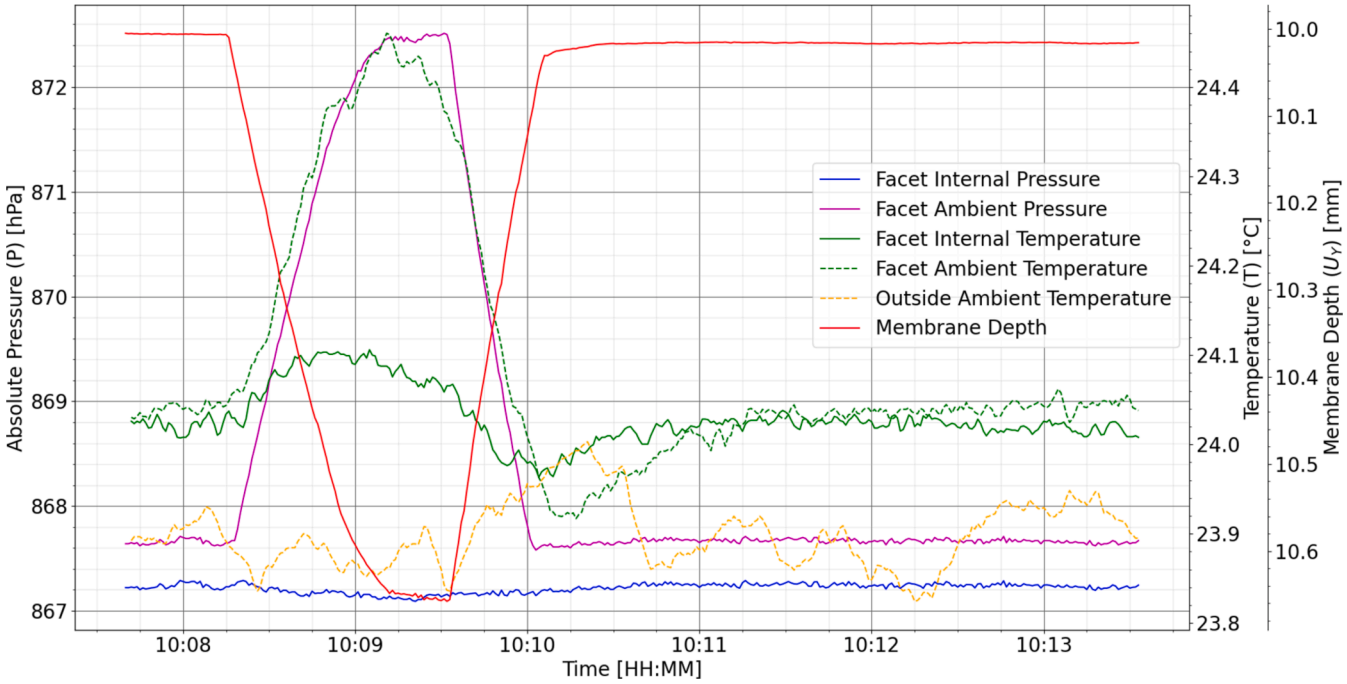

Fig. 26. Increase in ambient pressure test of Facet 4 (7 May 2023).

somewhat larger 12.7 % difference. The average internal temperature effect for the thicker membrane was 4.2 % lower than that of the thinner membrane. These differences between the two membrane thicknesses were minimal and likely due to the stiffness of the two thicknesses being slightly different.

When comparing the facets with different pretension levels (Facet 2, 3, and 4), where the lowest pretension was on Facet 4 (10.85 kg) and the highest pretension was on Facet 3 (80.88 kg), it was observed that the average ambient pressure effects on membrane depth were very similar for all facets, without a clear trend, as indicated in Table 2. The maximum difference between the highest value determined for Facet 2 (0.136 mm/hPa) and the lowest for Facet 3 (0.130 mm/hPa) was only 4.6 %. The impact of ambient temperature seemed to affect membrane displacement slightly less for the higher pretensioned facets. The highest pretension facet (Facet 3) resulted in an ambient temperature effect of 0.156 mm/C, while the lowest pretension (Facet 4) had an ambient temperature effect of 0.169 mm/C, resulting in a small difference of 8.3 %. However, the average internal temperature appeared to affect membrane displacement slightly more for the higher pretension facets, with the highest pretension facet (Facet 3) resulting in an internal temperature effect of 0.154 mm/C, compared to the lowest pretension (Facet 4) with an internal temperature effect of 0.144 mm/C,

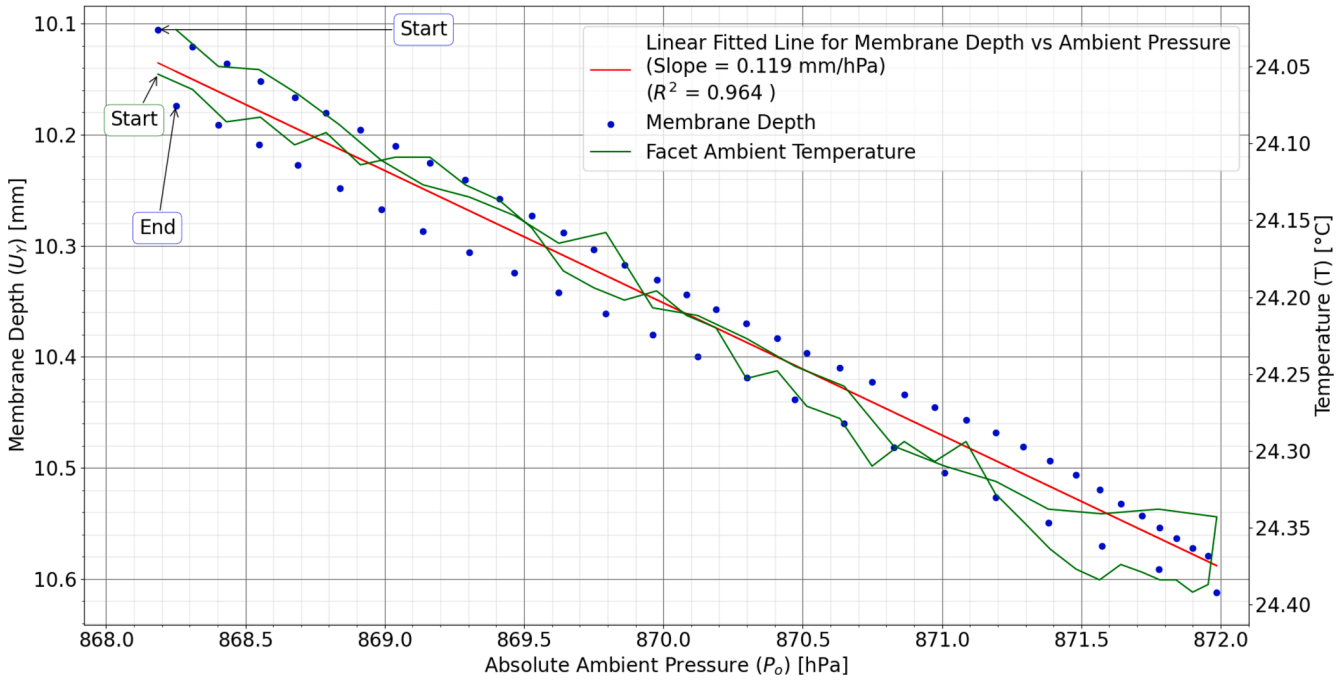

Fig. 27. Membrane depth and internal temperature of Facet 4 versus the increase ambient pressure (7 May 2023).

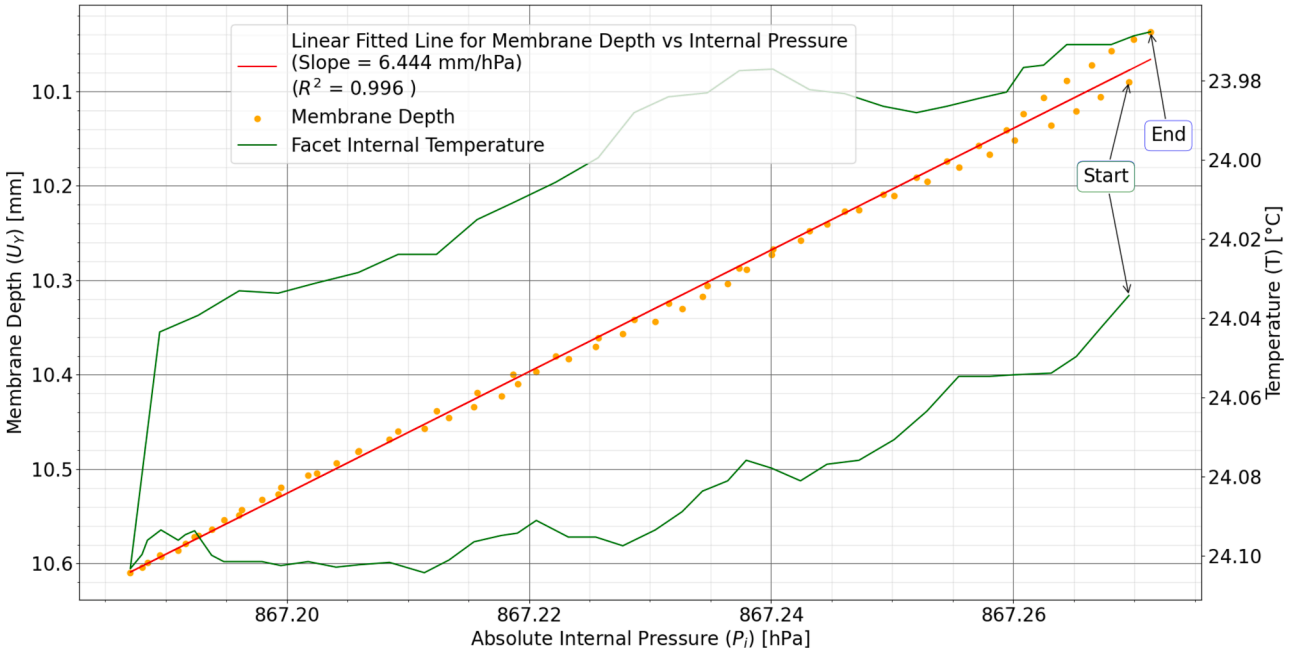

Fig. 28. Membrane depth and internal temperature versus internal pressure of Facet 4 as the ambient pressure increase (7 May 2023).

representing a modest difference of 6.9 %. Overall, these findings suggest that there were minor differences in how membrane displacement was affected by pretension variations ranging from about 10 kg to 80 kg. Nevertheless, in terms of ambient effects, the higher pretensioned facet resulted in less membrane displacement, which also had the lowest Et/T_o ratio of all five facets tested.

Furthermore, when comparing the differential pressure correlations with membrane displacement of the five facets, it is still evident that a small facet with high pretension and thin membrane would mitigate membrane displacement the best (see Table 3). However, when comparing differential temperature correlations with membrane displacement of the five facets, it was found that a small facet with a low pretension and thicker membrane would minimize membrane displacement. Since temperature effects are expected to govern membrane displacement during a typical operational day, it is recommended to further investigate the effects of differential temperature on the membrane displacement. As shown in Table 3, Facet 3 had a linear correlation of 2.365 mm/℃ between differential temperature and membrane displacement. However, the differential temperature was only about 1℃ for the entire constant rate of change cooling period, which means the membrane displacement was more related to the change in ambient pressure during this period. Therefore, when comparing the effects of differential temperature, it is recommended to maintain a constant direct ambient pressure during the test, as was

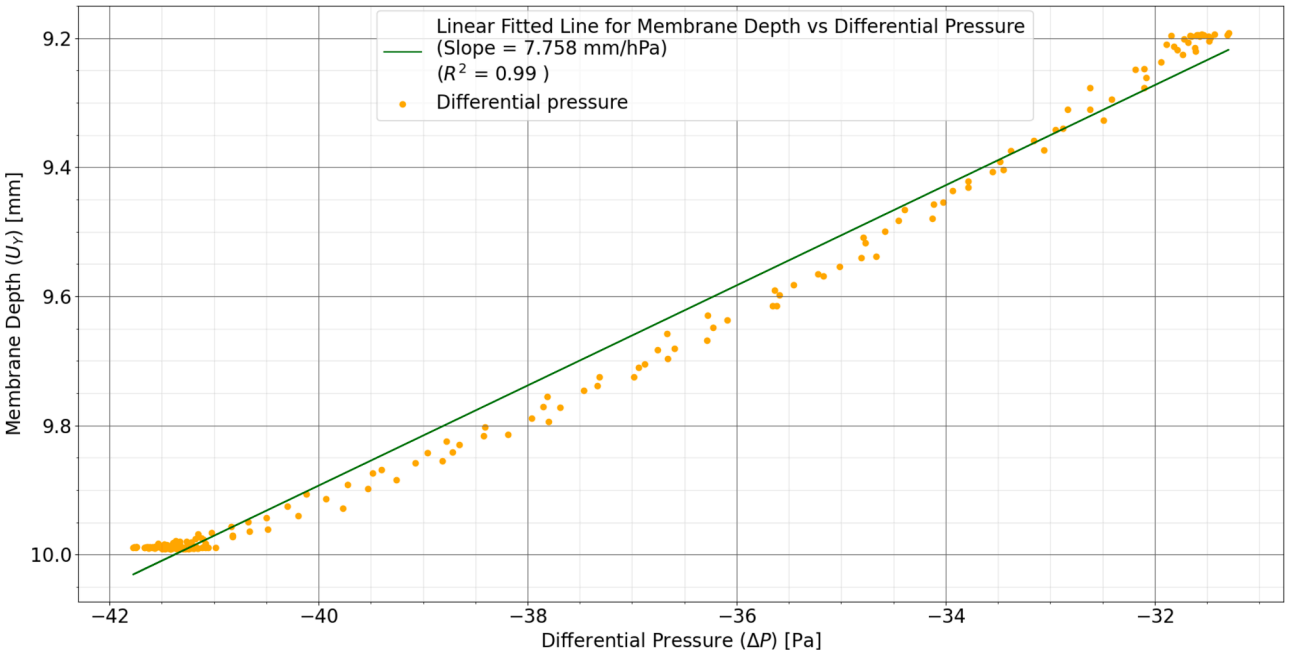

Fig. 29. Membrane depth versus differential pressure of Facet 4 as the ambient pressure decrease (7 May 2023).

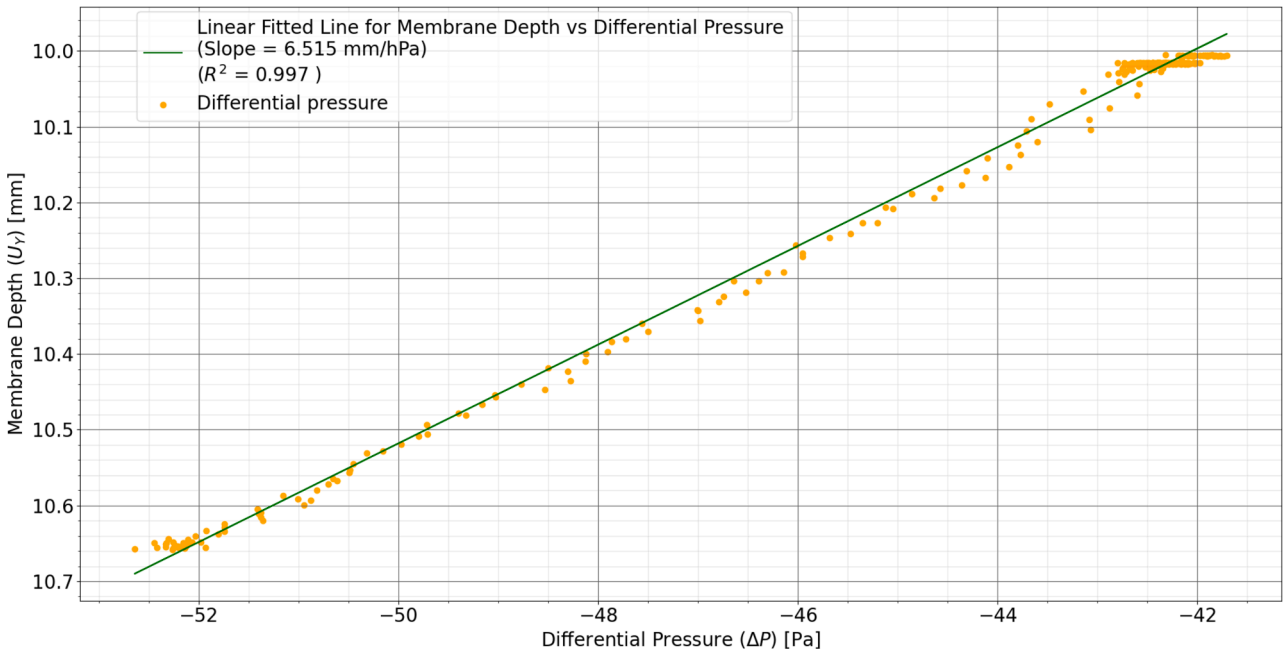

Fig. 30. Membrane depth versus differential pressure of Facet 4 as the ambient pressure increase (7 May 2023).

originally planned. However, the vacuum pump and high-pressure source were not effective enough in maintaining the pressure due to sudden changes caused by the heater switching on and off.

3.4. Outdoor experimental results

3.4.1. Outdoor test results without a focus control system

The outdoor test results for the uncontrolled facet demonstrated significant membrane displacement. During an operational day, the membrane depth decreased by a maximum of about 4 mm from an initial depth of 10 mm, as depicted in Fig. 38. The test began at around 7:30 in the morning when both the ambient temperature and pressure were on the rise. At approximately 10:15, the ambient pressure started to decrease while the ambient temperature continued to increase. By 14:15, the ambient temperature had peaked for the day at about 25 °C, and the ambient pressure began to rise again as the temperature decreased. The internal and ambient temperatures exhibited similarity throughout the day, indicating the presence of steady-state heat transfer conditions. Fig. 38 also reveals that the internal temperature of the facet had a substantial impact on membrane displacement, as evidenced by the nearly identical shapes of the two lines (red and green lines).

Since the facet was placed horizontally on the roof of a building, there was always a zenith angle throughout the day. Therefore, the membrane absorbed GHI, a combination of DNI and DHI. The GHI, measured from the SAURAN system [33], influenced the internal temperature throughout the day and the membrane displacement. Fig. 38

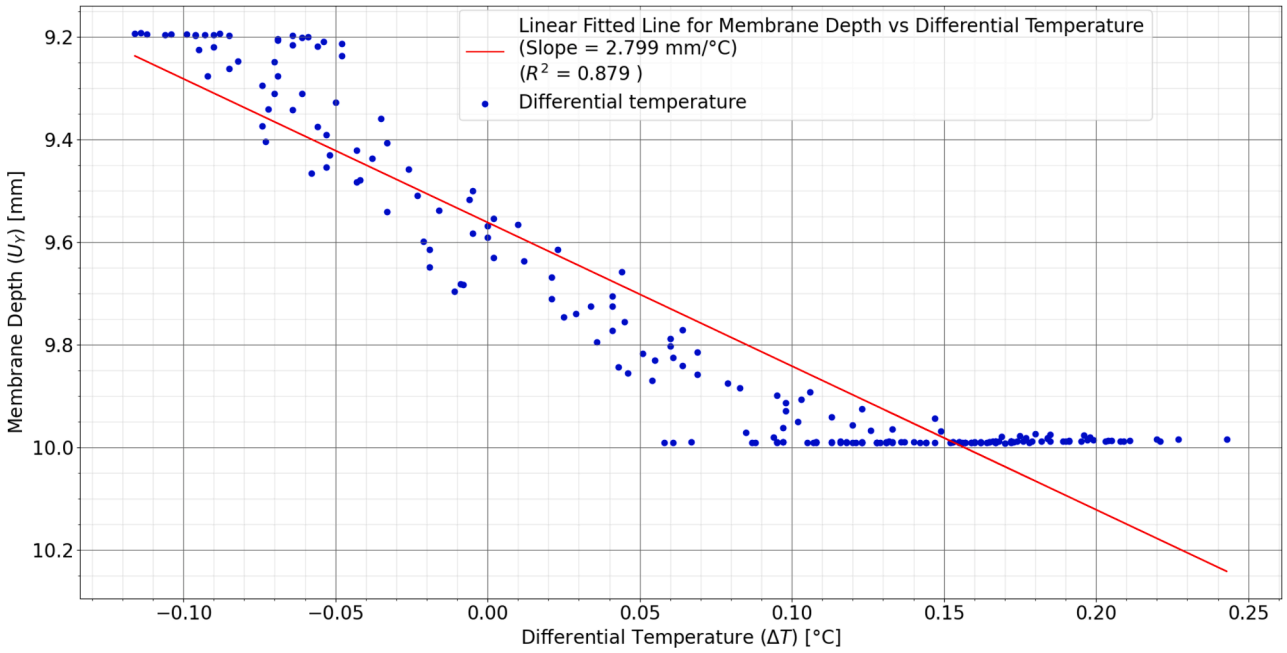

Fig. 31. Membrane depth versus differential temperature of Facet 4 as the ambient pressure decrease (7 May 2023).

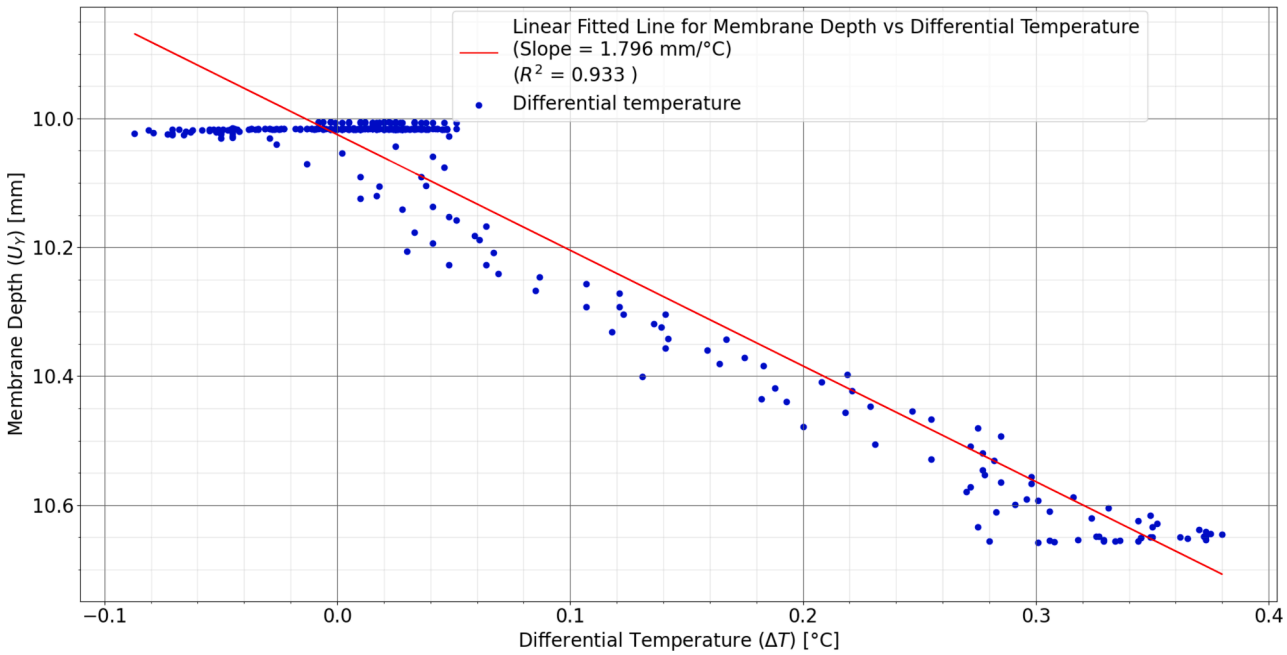

Fig. 32. Membrane depth versus differential temperature of Facet 4 as the ambient pressure increase (7 May 2023).

indicates that the internal facet temperature was affected by GHI in the morning as the radiation increased. Since the zenith angle was large at this point, the effects of DNI were minimal. At 11:30, the zenith angle was much smaller, and the effects of DNI were much higher with increasing DHI, which assisted in increasing the facet internal temperature until 14:00 when the solar radiation started to decrease gradually. This decrease in solar radiation and ambient temperature at the end of the day caused the facet internal temperature to decrease and the membrane depth to increase.

Fig. 39 shows that the wind velocity did not have a direct effect on membrane displacement. However, it is shown that the wind velocity did increase throughout the day with a sudden increase in velocity of about 1 m/s during the time when the GHI increased while the membrane depth remained constant at 7 mm (from 10:15 to 11:15). This indicates the influence of the wind: extracting heat from the membrane and effectively cancelling out the effect of the absorbed GHI, which would usually heat the facet internal air.

3.4.2. *Outdoor test results for a constant initial differential pressure*

From the outdoor test results of the controlled facet (see Fig. 40), where a constant differential pressure was maintained using a low-cost vacuum and air pump equipped with BMP280 barometric pressure sensors, it was evident that the membrane displacement was significantly lower throughout an operating day, compared to an uncontrolled facet reported by McGee and Le Roux [35] and indicated in Fig. 38 and Fig. 39. The membrane depth experienced an increase of about 1.6 mm

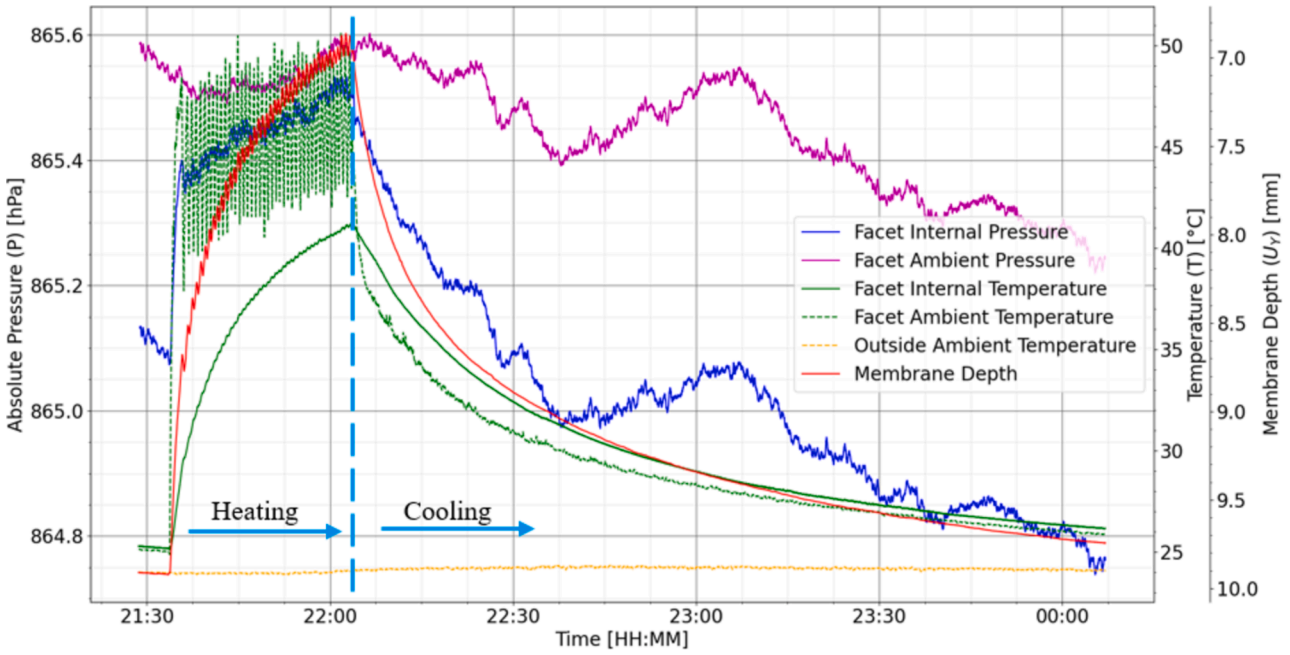

Fig. 33. Increase and decrease in ambient temperature test of Facet 4 (6 May 2023).

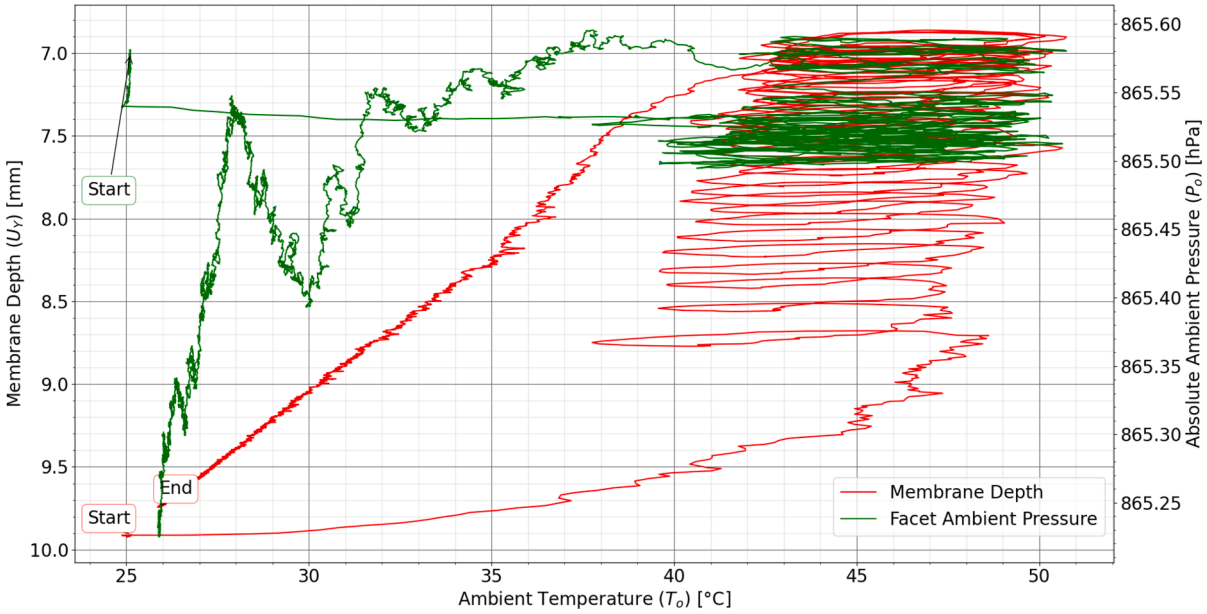

Fig. 34. Membrane depth and ambient pressure versus the ambient temperature of Facet 4 (6 May 2023).

and a decrease of about 0.8 mm. These fluctuations fell well within the required accuracy of ± 2 mm, as determined by Roosendaal et al. [22].

A 3-day duration test was also conducted to assess whether the effects of maintaining a constant differential pressure would work over an extended period, as depicted in Fig. 41. During this test, it was observed that the temperature increased each day, which was expected as the test was conducted near the end of winter. Additionally, there was a slight change in the maximum ambient pressure from the first day to the last day, with an increase towards the end of day three. Consequently, the fluctuation in membrane depth was not consistent across different days. However, it is noteworthy that the membrane depth remained within a relatively consistent range of between 11.9 mm and 13.5 mm every day between 6:00 and 18:00, with the depth remaining the same at 12:00 each day. This indicates that during the effective tracking time, the membrane depth was consistently maintained within a certain range. However, it may be necessary to reset the focus control system periodically, such as with the change of seasons or even more frequently based on the results of longer-duration tests.

In an ideal scenario, maintaining a constant differential pressure should result in a constant membrane depth. However, this assumption holds true only if the stiffness of the membrane material remains constant throughout a day. The properties of plastics, which make up the reflective membrane material, are significantly affected by temperature changes [33]. Specifically, polymer-based materials tend to exhibit higher stiffness at lower temperatures and lower stiffness at higher temperatures. In a controlled vacuum-membrane facet, where the internal gauge pressure was kept constant, the internal force exerted by the air particles on the membrane surface remained consistent. This

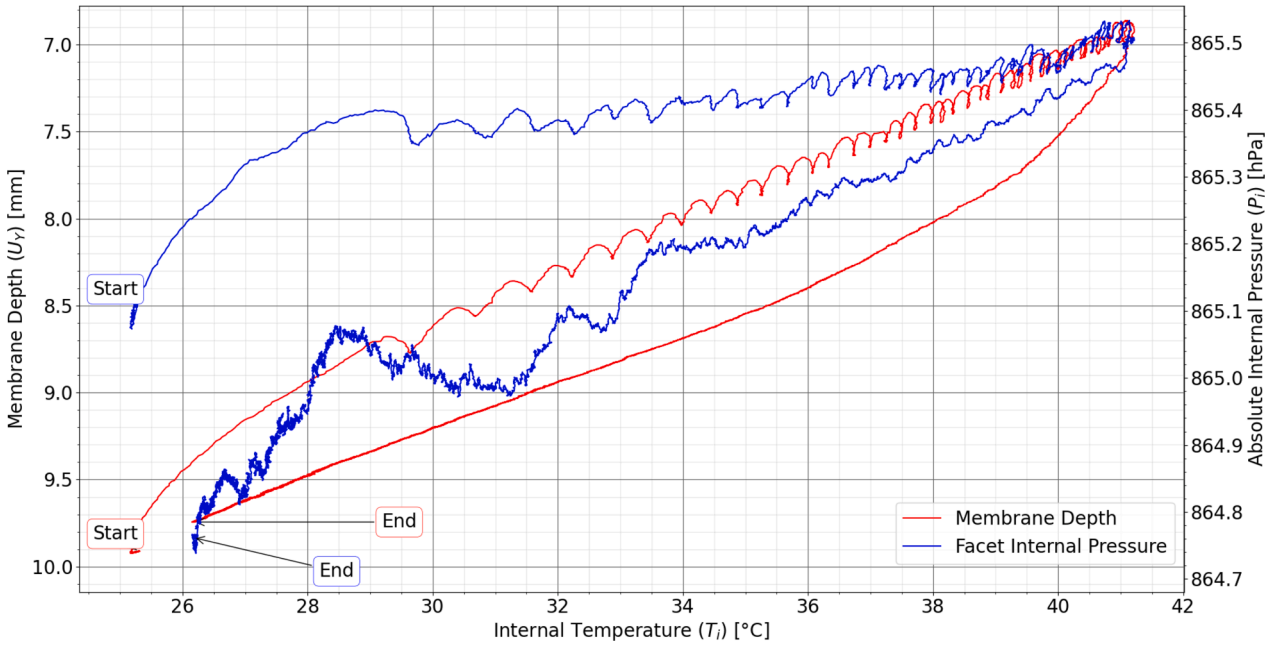

Fig. 35. Membrane depth and internal pressure versus the internal temperature of Facet 4 (6 May 2023).

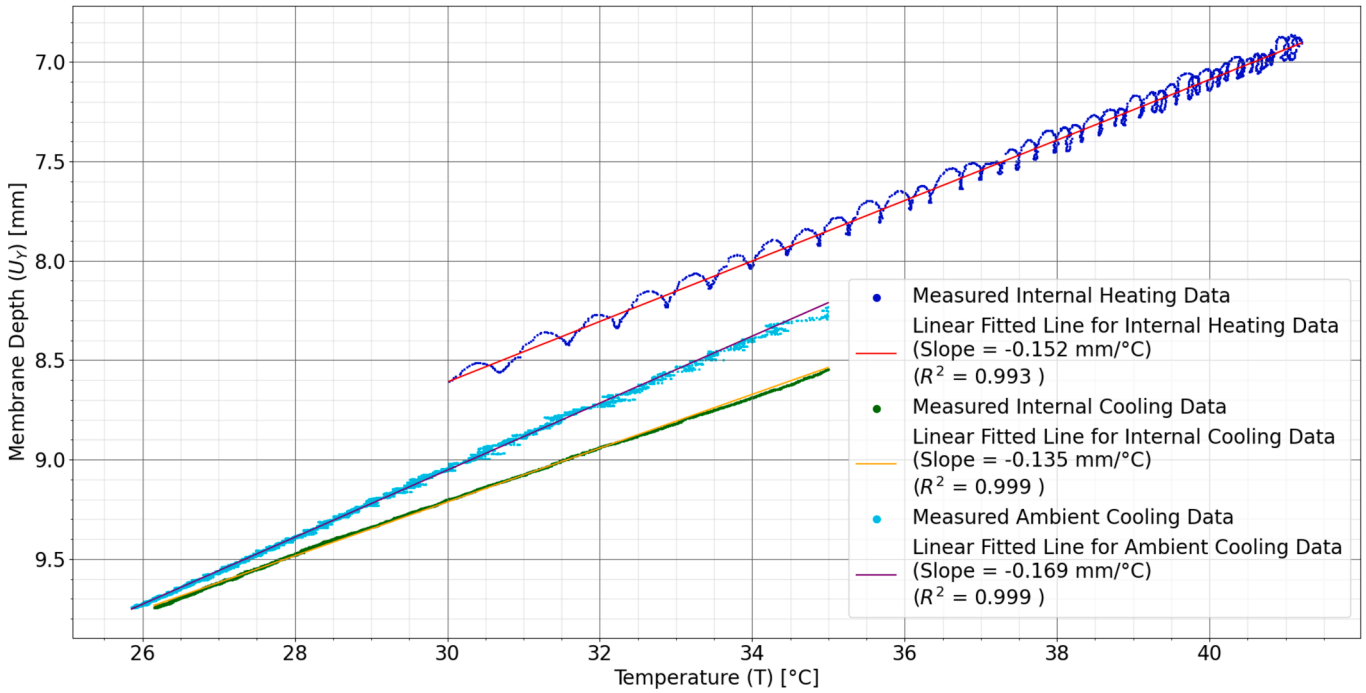

Fig. 36. Isolated linear trends of the membrane depth versus internal and external temperature of Facet 4 (6 May 2023).

internal force opposed the external force of the surrounding air particles and the stiffness of the material, which resulted in the characteristic parabolic concave shape of the vacuum-membrane facet. At lower temperatures, the external force from the surrounding air particles pushed against a stiffer membrane while the constant internal force remained the same. This led to the external force being less effective, causing the membrane to move upwards. Conversely, at higher temperatures, the external force pushed against a less stiff membrane while the constant internal force remained the same. Therefore, relying solely on differential pressure for a focus control system may not be effective for a polymer-based reflective membrane. In contrast, this approach could work for a metal-based membrane, like the one used in the SKI facet made with a 304 stainless steel membrane [24], because metal materials are not as sensitive to temperature changes within the given low range.

3.4.3. *Outdoor test results for a constant membrane depth*

In the outdoor test results of the controlled facet, where a constant membrane depth was maintained using a low-cost vacuum and air pump with the Hall effect module, it was successfully demonstrated that the membrane depth could be kept constant throughout a 12-hour test, as shown in Fig. 42. The membrane depth experienced small fluctuations,

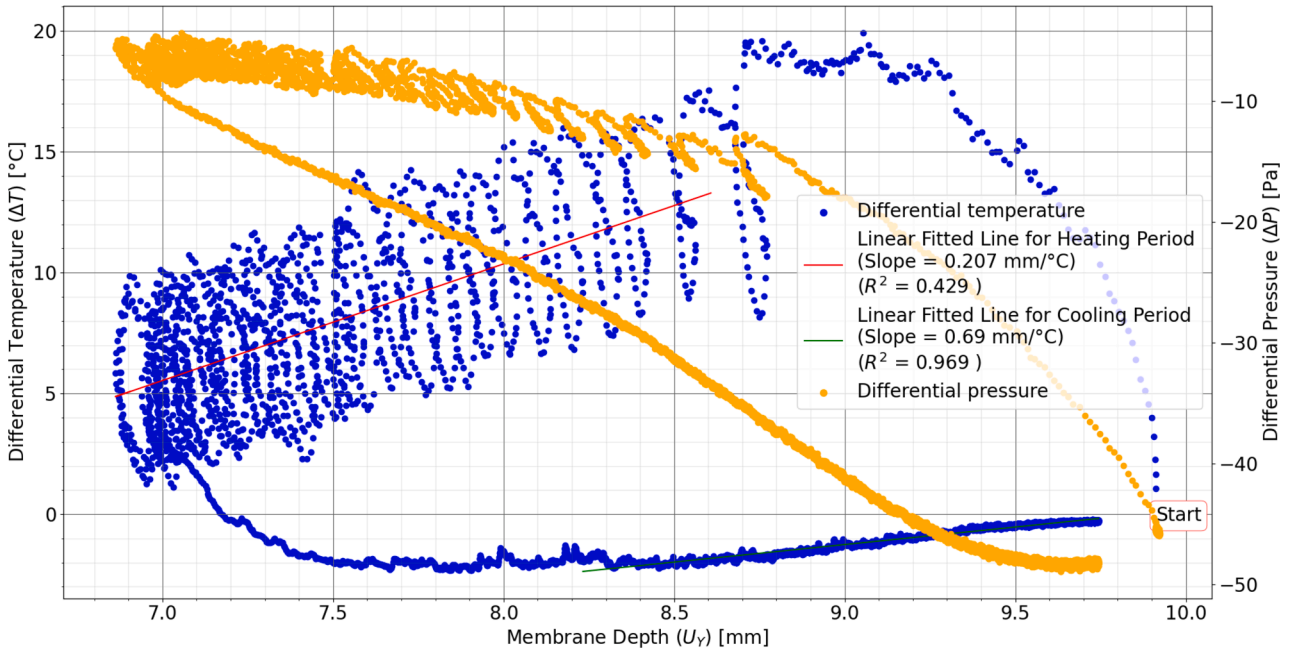

Fig. 37. Differential temperature and pressure versus membrane depth of Facet 4 (6 May 2023).

Table 3
Comparative summary of the controlled-environment differential pressure and temperature results of different facet types.

	Thin membrane	Large facet	Different pretension facets		
Facet	**1**	**5**	**4**	**2**	**3**
Satellite antenna size [cm]	75	80	75	75	75
Pretension [kg]	10.85	56.1	10.85	56.1	80.88
Thickness [mm] (with or without the removeable plastic layer)	0.095	0.1	0.1	0.1	0.1
Et/T_o ratio	6545	1709	8193	1584	1099
Membrane displacement per differential pressure change [mm/hPa] (decreased ambient pressure test)	9.713	10.08	7.758	6.096	6.299
Membrane displacement per differential pressure change [mm/hPa] increased ambient pressure test)	9.615	10.284	6.515	5.917	6.072
Average membrane displacement per differential pressure change [mm/hPa]	9.664	10.182	7.137	6.007	6.186
Membrane displacement per differential temperature change [mm/C] (ambient temperature heating period)	0.261	0.267	0.207	0.22	0.26
Membrane displacement per differential temperature change [mm/C] (ambient temperature cooling period)	1.034	1.555	0.690	0.772	2.365
Average membrane displacement per differential temperature change [mm/C]	0.648	0.911	0.449	0.496	1.313

with an increase of about 0.09 mm and a decrease of about 0.02 mm. These fluctuations fell well within the required accuracy of ± 2 mm, as determined by Roosendaal et al. [22] and is significantly smaller than the fluctuations that were reported in the previous section. This test result demonstrated that it was possible to maintain the desired membrane depth within a narrow range using the proposed depth sensing focus control system, and it is therefore recommended for further investigation and implementation.

3.5. Discussion

Experiments conducted in the controlled-environment enclosure on differently-manufactured vacuum-membrane facets showed that ambient temperature impacted the membrane displacement significantly more than ambient pressure throughout an operating day. It also revealed that a smaller facet would have less membrane displacement with altering static ambient conditions, compared to a larger facet with the same pretension and membrane thickness. A smaller facet would also result in a larger local f/D ratio, compared to a larger facet, which is preferred as this would result in a more optimal parabolic surface approximation according to Murphy and Tuan [13]. Furthermore, it was determined that a thinner membrane (without the removable plastic layer) and higher pretension would further reduce the membrane displacement caused by altering ambient conditions. This is also beneficial for an accurate parabolic approximation since a thin and high pretension membrane would further lower the Et/T_o ratio, as recommended by Murphy and Tuan [13] for a uniformly tensioned membrane. However, when comparing differential temperature correlations with membrane displacement, it was found that a small facet with a low pretension and thicker membrane would minimize membrane displacement. Nevertheless, it is important to note that these manufacturing techniques alone might not suffice to mitigate membrane displacement in the presence of dynamic ambient conditions, such as solar radiation, convection, and dynamic pressure due to wind, as noted from the outdoor experiments. The outdoor test results of a facet without a focus control system indicated that the ambient temperature and solar radiation primarily affected the internal temperature which affected the membrane depth. It was also noted that the wind velocity influenced the facet internal temperature since the membrane depth remained constant

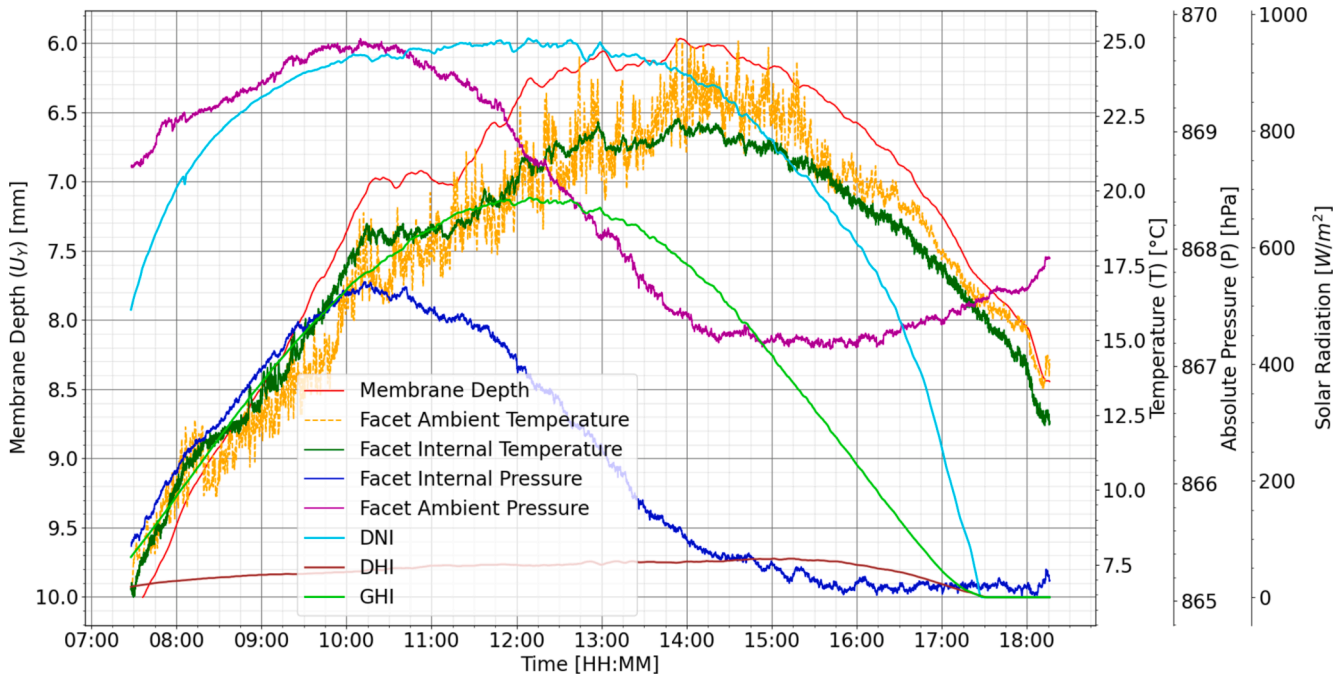

Fig. 38. Outdoor test results of Facet 4 without any focus control system (1 July 2023).

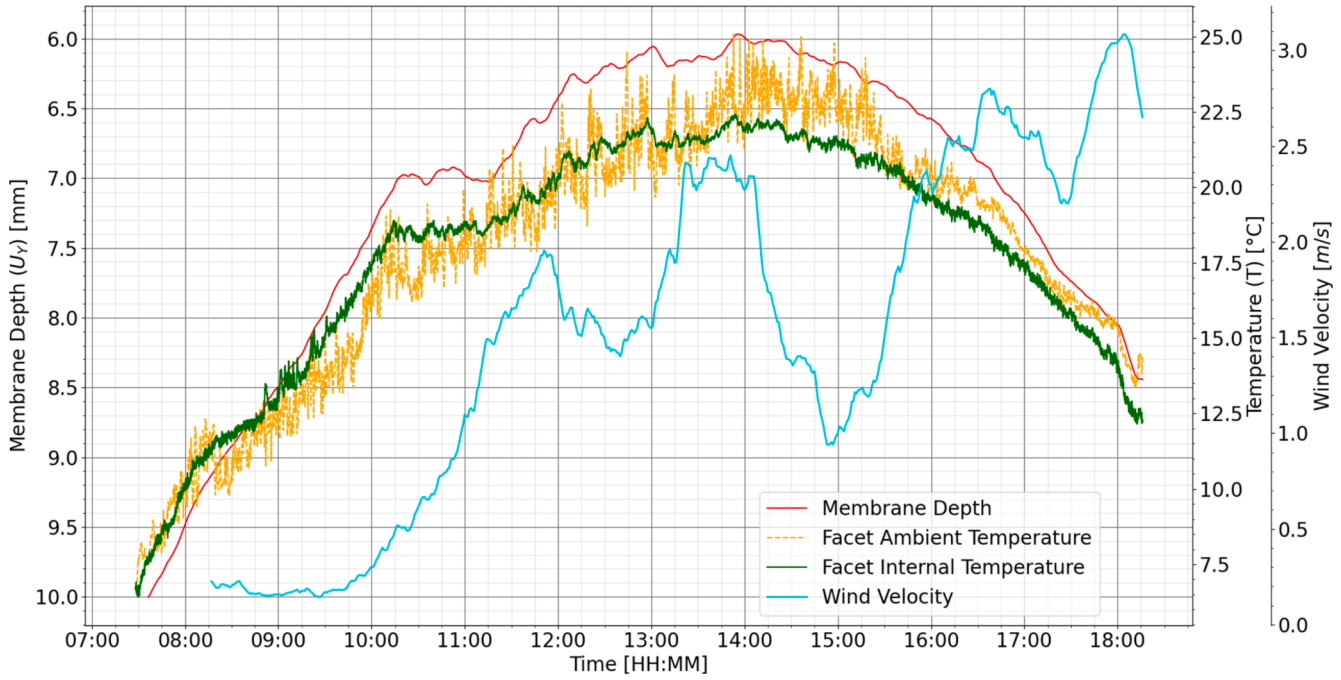

Fig. 39. Outdoor test results of Facet 4 including wind speed measured from the SAURAN system [33] (1 July 2023).

as the solar irradiance increased while the wind velocity increased. Addressing these dynamic effects requires the implementation of an active focus control system.

Outdoor experiments conducted on the focus control systems yielded significant insights. Firstly, maintaining a constant differential pressure for a vacuum-membrane facet was found to effectively reduce membrane displacement to within the required accuracy of ± 2 mm. This level of precision was crucial for achieving a targeted minimum intercept factor of 90 %, as stipulated by Roosendaal et al. [22] for a small-scaled CSP system such as ST-CHP [19]. However, even with this control in place, some residual membrane displacement persisted, which was suspected to be linked to the changing stiffness of the polymer-based membrane in response to temperature fluctuations. The focus control system equipped with a Hall-effect module actively monitoring membrane depth (suggested by Schertz et al. [24]), emerged as the most effective in eliminating membrane displacement, resulting in a total fluctuation of just 0.11 mm throughout an operating day.

The stiffness of the membrane was found to play a major role when attempting to maintain the differential pressure between the environment and inside of a facet to maintain the membrane depth. Relying solely on differential pressure control in a focus control system might not be suitable for a polymer-based reflective membrane due to its

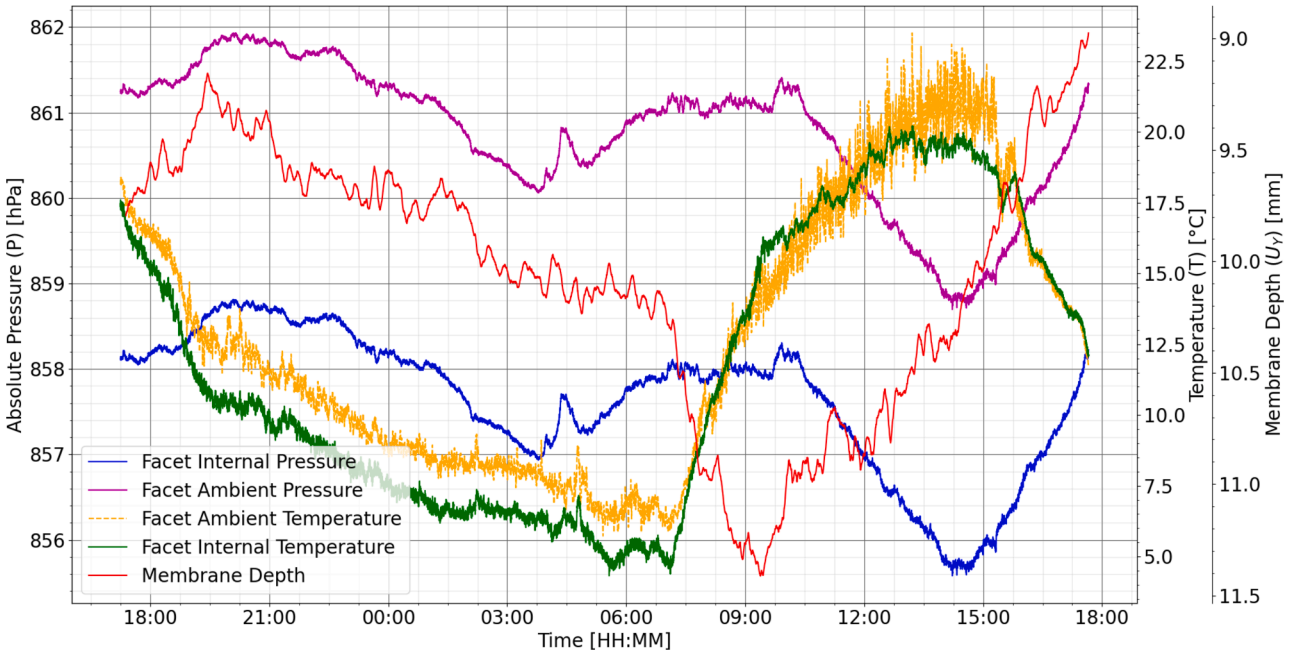

Fig. 40. Outdoor test results of Facet 4 with the constant differential pressure focus control system (8 July 2023).

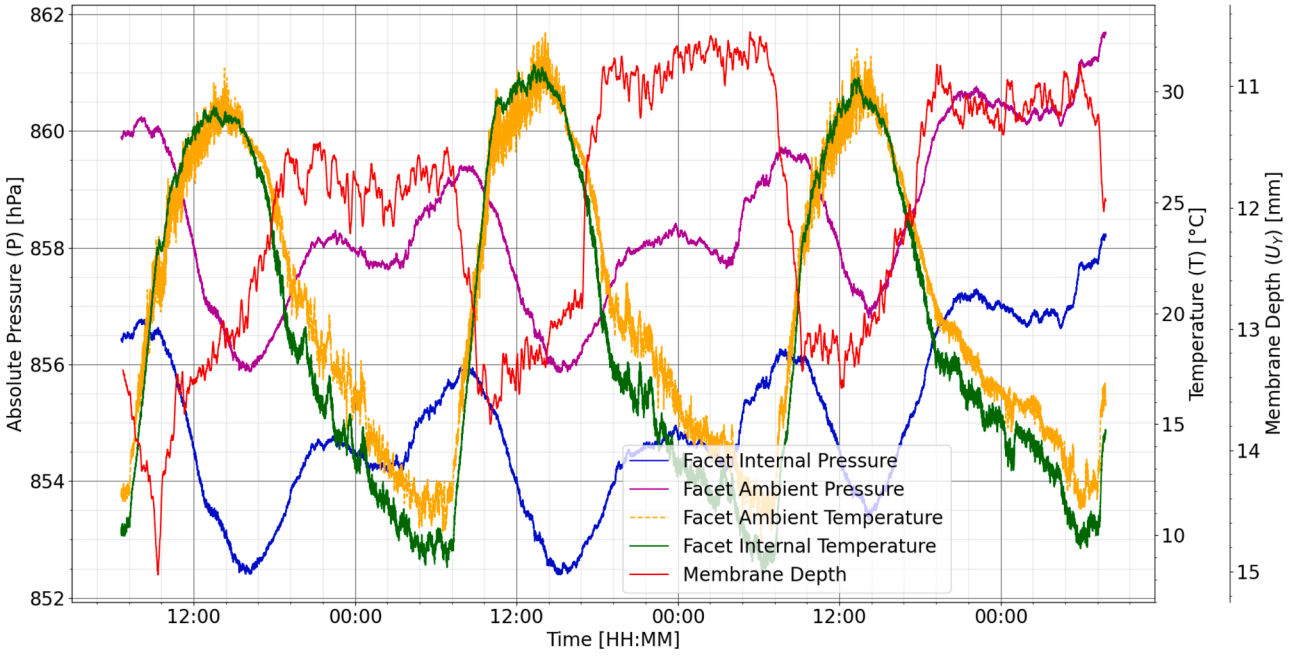

Fig. 41. Outdoor test results of Facet 4 with the constant differential pressure focus control system over 4 days (21 August – 24 August 2023).

sensitivity to temperature variations but could be the most cost-effective solution. Conducting additional material tests on the EverBright mirror film at various temperatures in accordance with ASTM D882 [26] would provide insights into how the differential pressure should be adjusted as ambient conditions cause fluctuations in membrane temperature.

4. Conclusion

The research considered the prospects of a multifaceted vacuum-membrane solar dish concentrator, in terms of its manufacturing, operation, performance and control. The membrane displacement of a vacuum-membrane solar dish facet is highly affected by the change in ambient conditions throughout a typical operational day. This affects the focal lengths of the facets in a multifaceted solar dish arrangement, which ultimately reduces the optical efficiency of the solar-dish concentrator. New manufacturing techniques were therefore pursued in this work together with low-cost focus control systems in order to mitigate membrane displacement. Different levels of membrane pre-tension, with and without the removable plastic layer, as well as two different facet sizes (75 cm and 80 cm) were considered in indoor tests. Two different control systems were also investigated in outdoor tests.

The focus control system equipped with a Hall-effect module actively monitoring membrane depth, emerged as the most effective in eliminating membrane displacement, resulting in a total fluctuation of just

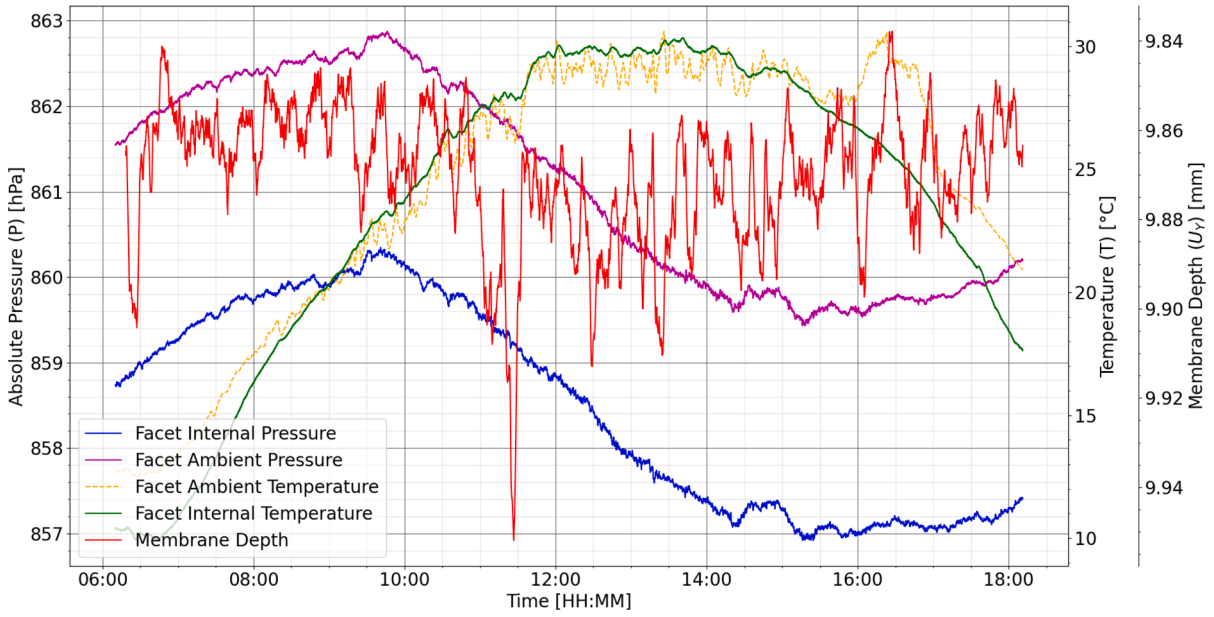

Fig. 42. Outdoor test results of Facet 4 with the constant membrane depth focus control system (14 August 2023).

0.11 mm throughout an operating day. This level of stability and opting for a small facet with a thin membrane and high pretension will ensure that the facet maintains a consistent optical performance during operation, ultimately advancing the reliability and efficiency of low-cost vacuum-membrane technology. The results were supported by material tests to determine the Young's modulus of the material as well as a finite element analysis, showing a 4.7 % error in membrane depth when compared to the measured displacement.

5. Recommendations

The following recommendations can be made from the study:

- A recommendation for future work would be to determine how dynamic pressure due to wind could affect membrane displacement by measuring wind velocity as close as possible to the experimental setup with the same elevation. In the current work, the SAURAN system was about 25 m higher in elevation, and therefore the wind speed and direction could have been different from what was present at the experimental setup.
- The experimental work that was presented in the current study could assist in building and validating future analytical models of the elliptical vacuum-membrane solar dish. However, developing a computational fluid dynamics (CFD) model, incorporating membrane material properties obtained from tensile tests along with solar radiation and convection parameters, could be a better modelling approach due to the complex geometries and conditions.
- More accurate piecewise functions or other functions can be investigated in future work to describe the effect of temperature on the membrane depth.
- Conducting additional material tests on the EverBright mirror film at various temperatures would provide insights into how the differential pressure should be adjusted as the ambient conditions cause fluctuations in membrane temperature.
- When comparing the effects of differential temperature, it is recommended to conduct further investigations, since the vacuum pump and high-pressure source were not effective in maintaining the pressure due to sudden changes caused by the heater switching on and off.
- Lastly, it is recommended for the facet to actively track the sun if outdoor tests are to be performed as it could yield more realistic data.

Declaration of competing interest

The authors declare the following financial interests/personal relationships which may be considered as potential competing interests: MCGEE DS, LE ROUX WG, Pending Patent, "A position sensor and focus control system". Reference Number: 2024/06700.

Acknowledgements

The authors express their gratitude to the Renewable Energy Hub and Spokes Program of the Department of Science and Innovation (DSI) for financial support through the UP Solar Thermal Spoke.

Data availability

Data will be made available on request.

References

[1] L.M. Murphy, Technical and Cost Potential for Lightweight, Stretched-Membrane Heliostat Technology (SERI/TP-253-2079), Las Vegas, 1984.
[2] J.K. Swanepoel, W.G. Le Roux, C. Roosendaal, S.H. Madani, G. De Wet, T. Nikolaidis, W. Roosendaal, C. Onorati, A. Sciacovelli, Y. Liu, T.S. Mokobodi, D. S. McGee, K.J. Craig, Initial experimental testing of a hybrid solar-dish Brayton cycle for combined heat and power (ST-CHP), Appl. Therm. Eng. 249 (2024), https://doi.org/10.1016/j.applthermaleng.2024.123275.
[3] R. Gee, "Sundog Solar Technology," 2023. [Online]. Available: https://www.sundogsolartech.com/. [Accessed 16 September 2023].
[4] R.C. Gee, Development of an Abrasion-Resistant Antisoiling Coating for Front-Surface Reflectors, DOE/EERE Solar Technologies Office, Arvada, 2017.
[5] S.V. Starodubtsev, G.Y. Umarov, N.V. Kordub, A 2.7-meter diameter vacuum film solar concentrator, Geliotekhnika 1 (1965) 16.
[6] J. Coventry, C. Andraka, Dish systems for CSP, Sol. Energy 152 (2017) 140–170, https://doi.org/10.1016/j.solener.2017.02.056.
[7] D.J. Alpert, T.R. Mancini, R.M. Houscr, J.W. Grossman, P. Schissel, M. Carasso, G. Jorgensen, M. Scheve, Solar concentrator development in the United States, Solar Energy Mater. 24 (1991) 307–319, https://doi.org/10.1016/0165-1633(91)90071-R.
[8] T.R. Mancini, Analysis and design of two stretched-membrane parabolic dish concentrators, J. Sol. Energy Eng. 113 (3) (1991) 180–187, https://doi.org/10.1115/1.2930490.
[9] M. Schmitz, G. Ambrosetti, A. Steinfeld, T. Cooper, On-sun optical characterisation of a solar dish concentrator based on elliptical vacuum membrane facets, Sol. Energy 153 (2017) 732–743, https://doi.org/10.1016/j.solener.2017.06.009.
[10] F. Dähler, G. Ambrosetti, J.A. Montoya-Zegarra, K. Schindler, A. Steinfeld, High-concentration solar dishes based on pneumatic reflecting membranes, Sol. Energy 124 (2016) 89–100, https://doi.org/10.1016/j.solener.2015.11.021.
[11] W. Flügge, Stresses in Shells, Springer-Verlag, New York, 2013.

[12] O. Frei, Tensile structures, MIT Press, Cambridge, 1982.
[13] L. M. Murphy, C.Y. Tuan, The formation of optical membrane reflector surfaces using uniform pressure loading, Solar Energy Research Institute, Report Number SERI/TR-253-3025, Golden, 1987, 10.2172/6212416.
[14] K. Gehlisch, H. Heikal, A. Mobarak, M. Simon, Large parabolic dish collectors with small gas-turbine, stirling engine or photovoltaic power conversion systems, Los Angeles, 1982(a).
[15] K. Gehlisch, Small solar power plants with large parabolic dish collector, Berlin, 1982(b).
[16] B.H. Khoshalm, 50-kW solar membrane concentrator, in: 4th SOLERAS Workshop, Kansas City, 1983.
[17] L.M. Murphy, Moderate axisymmetric deformations of optical membrane surfaces, J. Sol. Energy Eng. 109 (2) (1987) 111–120, https://doi.org/10.1115/1.3268187.
[18] C. Roosendaal, J.K. Swanepoel, W.G. Le Roux, Performance analysis of a novel solar concentrator using lunar flux mapping techniques, Sol. Energy 206 (2020) 200–215, https://doi.org/10.1016/j.solener.2020.05.050.
[19] J.K. Swanepoel, W.G. Le Roux, A.S. Lexmond, J.P. Meyer, Helically coiled cavity receiver for a micro-scale direct generation steam Rankine cycle using novel solar dish design, Appl. Therm. Eng. 185 (2019) 116427, https://doi.org/10.1016/j.applthermaleng.2020.116427.
[20] D.S. McGee, W. Roosendaal, W.G. Le Roux, Environmental investigation of vacuum-membrane solar-dish facets, in AIP Conference Proceedings (Presented at the 27th SolarPACES conference 27 September–1 October 2021), Online, 2023, 10.1063/5.0149745.
[21] J.K. Swanepoel, C. Roosendaal, W.G. Le Roux, Photogrammetry analysis of a vacuum-membrane solar dish using elliptical television antennas, in: AIP Conference Proceedings 2445, 120021 (Presented at the 26th SolarPACES conference 28 September–2 October 2020), Freiburg (Online), 2022, 10.1063/5.0087025.
[22] C. Roosendaal, J.K. Swanepoel, W.G. Le Roux, Optical modelling of a vacuum-membrane solar dish based on elliptical television antenna, in: Southern African Sustainable Energy Conference (SASEC2021), Stellenbosch, 2021 (17 - 19 November 2021).
[23] SAIC, Facet Development for a Faceted Stretched-Membrane Dish by SAIC; SAND91 - 7008, Sandia National Laboratories, Albuquerque, 1991.
[24] P. T. Schertz, D.C. Brown, A.I. Konnerth, Facet development for a faceted stretched-membrane dish by solar kinetics Inc.; SAND91-7009, Sandia National Laboratories, Albuquerque, 1991.
[25] J. W. Grossman, R. M. Houser and W. W. Erdman, "Testing of the Prototype Facets for the Stretched-Membrane Faceted Dish," Sandia Natlonal LaboratorlH, Albuquerque, New Mexico, 1991.
[26] ASTM International, Standard Test Method for Tensile Properties of Thin Plastic Sheeting, ASTM International, West Conshohocken, 2010, 10.1520/D0882-10.
[27] B.J. Goodno, J.M. Gere, Mechanics of Materials, 9th ed., Canada: Cengage Learning, ISBN: 978-1-337-09335-4, 2016.
[28] SolidWorks, "SolidWorks," 2024. [Online]. Available: https://www.solidworks.com/. [Accessed 07 January 2024].
[29] SolidWorks-Help, "Dassault Systems," 2023. [Online]. Available: https://help.solidworks.com/2023/english/SolidWorks/sldworks/r_welcome_sw_online_help.htm. [Accessed 26 August 2023].
[30] DuPont Teijin Films, "Technical information," 2003. [Online]. Available: https://usa.dupontteijinfilms.com/wp-content/uploads/2017/01/Mylar_Physical_Properties.pdf. [Accessed 16 September 2023].
[31] Ellies Electronics, "Elsat 75cm Dish – Ellies Electronics," 2023. [Online]. Available: http://e-systems.co.za/System/FabSheets/0DE75.pdf. [Accessed 30 October 2023].
[32] Ellies Electronics, "Elsat 80cm Dish – Ellies Electronics," 2023. [Online]. Available: http://e-systems.co.za/System/FabSheets/0DL80.pdf. [Accessed 30 October 2023].
[33] M. Brooks, S. du Clou, J. van Niekerk, P. Gauche, C. Leonard, M. Mouzouris, A. Meyer, N. van der Westhuizen, E. van Dyk, F. Vorster, SAURAN: a new resource for solar radiometric data in Southern Africa. Energy in Southern Africa 26 (2015) 2-10, 2015, 10.17159/2413-3051/2015/v26i1a2208.
[34] Bosch Sensortec, "BMP280 Digital, barometric pressure sensor," August 2012. [Online]. Available: https://www.bosch-sensortec.com/media/boschsensortec/downloads/product_flyer/bst-bmp280-fl000.pdf. [Accessed 29 May 2024].
[35] D.S. McGee, W.G. Le Roux, Controlled static enviroment tests on vacuum-membrane solar-dish facets for a low-cost vacuum control system, in: Presented at the ISES Solar World Congress (SWC23) 30 October - 4 November 2023, New Delhi, 2024, 10.18086/swc.2023.03.08.